Quantitative prediction of the modulation behavior of twisted nematic liquid crystal displays based on a simple physical model

A. Márquez

Departamento de Física, Universidad Autónoma de Barcelona, 08193 Bellaterra, Spain

C. Iemmi

Departamento de Física, Facultad de Ciencias Exactas y Naturales, Universidad de Buenos Aires, 1428 Buenos Aires, Argentina

I. Moreno

Departamento de Ciencia y Tecnología de Materiales. Universidad Miguel Hernández. 03202 Elche, Spain

J. A. Davis

Department of Physics, San Diego State University, San Diego, California 92182

J. Campos and M. J. Yzuel

Departamento de Física, Universidad Autónoma de Barcelona, 08193 Bellaterra, Spain

Abstract

A method to perform a predictive search for a given amplitude and phase modulation response in twisted nematic liquid crystal displays is presented. The algorithm is based on a simple physical model that we recently proposed and that considers the effect of liquid crystal layers located in the vicinity of the edges, which are not capable to tilt. This model was demonstrated to explain accurately the experimental transmittance modulation curves. Here the model is applied to perform a predictive search for an optimized modulation by changing the input and output polarization configuration. A generalized configuration to generate and detect elliptically polarized light is proposed. The method is applied for searching two different configurations useful for optical image processors: phase-only modulation and amplitude-only modulation. The excellent agreement with the experimental measurements validates the potentiality of the proposed method.

1.- Introduction

Twisted nematic liquid crystal displays (LCD) have been widely used as spatial light modulators (SLM) and programmable optical devices [1,2]. In general they produce coupled amplitude and phase modulation versus the applied voltage [3]. This coupling effect deteriorates the response of ideal optical elements which are designed as phase-only or amplitude-only functions. This coupling effect may be reduced by the design of elements adapted to the restricted coding domain of SLMs [4,5]. Another approach consists in looking for the configuration of polarizing elements that optimizes the behavior of the SLM as phase only modulator or as amplitude only modulator.

In order to look for an optimum configuration it is very useful to have a physical model for the LCD where the amplitude and phase modulation introduced by the LCD can be predicted with a good accuracy. In this sense a realistic physical model for the LCD based on the elastic properties of the liquid crystal molecules was proposed by Berreman [6,7]. This model was used by Taber et al [8] to study the transmittance of a liquid crystal light valve LCLV. The knowledge of the physical parameters of the liquid crystal material has been used to calculate the director profiles to considerably accuracy [9]. They permit to perform accurate numerical simulations of the LCD optical response, useful for the design of the displays [10].

During the last decade, advances in the technology made LCDs commercially available devices for other applications. In particular LCDs extracted from videoprojectors have been widely used to build real-time optical image processors [11,12]. In this case, the researcher does not have information about the internal physical properties of the display, and it is forced to perform an external calibration.

In this sense, Lu and Saleh [13] proposed a simplified model based on the Jones matrix formalism, which has been widely used in previous attempts to make a quantitative prediction of the modulation of the LCD. In ref. [12] Gonçalves-Neto *et al* made a search for a phase-mostly configuration by changing the angles of input and output polarizers. In ref. [14], Yamauchi and Eiju also applied the Lu and Saleh model to optimize the angles of the polarizers

based on a numerical simulation. The model proposed by Lu and Saleh has been proved to be a simple and good approximation for the device. However it is not accurate enough to describe the complex transmittance modulation for thin displays. An improved physical model was introduced by Coy et al [15].

Recently we presented a model to describe the optical properties of the LCD based on the Jones matrix theory [16]. This model assumes two free parameters that change with the applied voltage: 1) the effective birefringence of the liquid crystal molecules capable to tilt, which are located in the central part of the panel, and 2) the birefringence of the edge layers, which can not tilt. This model has been shown to lead to excellent agreement with the experiments.

In the last years the manufacturing of LCDs have evolved into the production of devices with a larger number of pixels that are thinner to achieve higher operating speeds. Davis et al [17] demonstrated that the use of the eigenvectors [18] of the LCD results in a great improvement in phase-only modulation with respect to the case in which only linearly polarized light is considered. Moreno *et al.* [19] demonstrated the experimental feasibility of the eigenvectors in order to obtain phase-only modulation with a thin LCD. In order to generate and detect the eigenvectors quarter wave-plates were placed in front of and behind the LCD with their extraordinary axis parallel to the director axis of the LCD at the input and at the output respectively. The display industry have been integrating waveplate layers in reflective LCDs to improve the viewing angle properties (commonly referred as compensating films). In our case we place two external waveplates, in order to control the polarization before and behind the LCD.

In this paper we apply our quantitative model to perform a predictive search for a desired operating curve of a LCD operating in transmissive mode. In particular, phase-only and amplitude-only modulations are desired configurations for applications as programmable optical devices in image processors and in applications in diffractive optics. We use the most general configuration possible of the polarizing elements to generate and detect elliptically polarized

light: the extraordinary axis of the waveplates can have any orientation with respect to the director axis of the LCD and the waveplates introduce arbitrary retardance. In this way we have more degrees of freedom to look for the desired amplitude or phase modulation. The eigenvectors of the LCD are one particular case of the elliptically polarized light that we can generate and detect with the proposed general configuration of the polarizing elements.

In the simulations we have been able to predict configurations which show an almost perfect phase-only modulation or and almost perfect amplitude-only modulation with the thin LCD we are working. The excellent agreement of the experimental results with the ones predicted by the simulation validate the proposed approach. In the next Section we review the physical model we recently proposed to describe the physical properties of the LCD.

2.- Jones theory for liquid crystal displays

We consider the LCD as divided in three different parts. Figure 1 shows an scheme of the assumptions made by the model. In the central part of the display the twist angle changes linearly with the depth of the cell and the difference of refractive index (Dn) is constant. When a voltage is applied through the electrodes of the display, the liquid crystal molecules tilt towards the direction of propagation (z axis). This causes a change in Dn. This part fulfills the assumptions made by Lu and Saleh [13]. However, in general those liquid crystal layers close to the surfaces are not capable to tilt and to twist the same amount as those in the central part do. A better approximation for this situation was proposed by Coy *et al* in ref. [15]. They considered these layers that do not tilt as two wave-plates coated to the surfaces, and oriented with its extraordinary axis parallel to the liquid crystal director at the input face and at the output face respectively. In these layers they assumed that the twist angle remains constant and Dn does not change with the voltage. Let us assume that the edge layers have a thickness d_1 while the central part has a thickness d_2. The total thickness of the display is $d=2d_1+d_2$. In figure 1, the assumptions considered for the three parts are sketched, for twist angle and Dn.

Recently we proposed a variation of the model by Coy *et al* by assuming that the thicknesses of these layers are variable, i.e, d_1 and d_2, change with the voltage [16]. With this assumption we could obtain excellent agreement between theory and experimental modulation curves. We remark that the attractive features of the model we proposed are its simplicity while providing a high degree of accuracy.

The Jones matrix $\mathbf{M_{LCD}}$ that describes the LCD assuming this model depends on three parameters:

1) The twist angle α that the liquid crystal molecules describe from the input to the output surface. This parameter is fixed during the fabrication of the display.
2) The birefringence $\beta(\mathrm{V})$ of the central part of the display which is defined as $\beta(\mathrm{V}) = \pi d_2(\mathrm{V})\Delta n(\mathrm{V})/\lambda$. This parameter changes with the voltage V in two ways. First the thickness d_2 decreases as the voltage increases, and second Δn decreases as voltage increases.
3) The birefringence $\delta(\mathrm{V})$ of the edge layers, defined as $\delta(V) = \pi d_1(V)\Delta n/\lambda$. This parameter changes because the thickness d_1 increases with voltage.

If the laboratory coordinates system has its *x*-axis parallel to the liquid crystal director at the input surface of the display, the Jones matrix that describes the device is given by [13]

$$\mathrm{M_{LCD}}(\alpha,\beta,\delta) = exp(-i(\beta+2\delta))\mathrm{R}(-\alpha)\begin{bmatrix} X-iY & Z \\ -Z & X+iY \end{bmatrix} \qquad (1)$$

where

$$X = cos\gamma cos2\delta - \frac{\beta}{\gamma} sin\gamma sin2\delta, \qquad (2a)$$

$$Y = cos\gamma sin2\delta + \frac{\beta}{\gamma} sin\gamma cos2\delta, \qquad (2b)$$

$$Z = \frac{\alpha}{\gamma}\sin\gamma, \qquad (2c)$$

$\gamma = \sqrt{\alpha^2 + \beta^2}$ and $\mathbf{R}(\theta)$ is the two dimensional rotation matrix, i.e.

$$\mathrm{R}(\theta) = \begin{bmatrix} cos\,\theta & sin\theta \\ -sin\theta & cos\,\theta \end{bmatrix} \tag{3}$$

We used previously discussed techniques [20,21,22] to measure the orientation of the director axis angle at the entrance face Ψ_D, the twist angle α and the value of the birefringence when the LC cell is in the off state, β_{OFF}. In the off state $\delta(V)$ tends to be zero and β_{OFF} may be considered as the maximum birefringence the display can reach. In our experiments we use a Sony LCX012BL twisted nematic LCD extracted from a Sony videoprojector model VPL-V500. The parameters obtained for this display are: $\alpha = -92$ degrees, $\Psi_D = +46$ with respect to the vertical laboratory axis, and $\beta_{OFF} = 231$ degrees for a wavelength $\lambda = 458\,nm$ from an Argon laser.

3.- Characterization of the display

In ref [16] we proposed a method to evaluate the values of $\beta(V)$ and $\delta(V)$. It is based on a fitting procedure of experimental intensity transmission curves using the model described in the previous section. In the following the coordinates system is taken in such a way that the x axis coincides with the director of the SLM at the input face. The angles of the elements in front of the SLM are taken with respect to the director at the input face, and the angles of the elements behind the SLM are taken with respect to the director at the output face. The normalized transmission of the LCD inserted between two polarizers with transmission axis at angles φ_1 and φ_2 is given by

$$T_{(\varphi_1,\varphi_2)} = [X\,cos(\varphi_1 - \varphi_2) + Z\,sin(\varphi_1 - \varphi_2)]^2 + [Y\,sin(\varphi_1 + \varphi_2)]^2 \tag{4}$$

Three configurations of the polarizers were used to fit experimental transmission curves, (φ_1=0, φ_2=+90), (φ_1=+45, φ_2=-45) and (φ_1=+22.5, φ_2 =+112.5). They lead to the following expressions for the normalized transmission

$$T_{(0,90)} = \frac{\alpha^2}{\gamma^2} sin^2 \gamma, \tag{5}$$

$$T_{(45,-45)} = 1 - \left(cos\gamma cos 2\delta - \frac{\beta}{\gamma} sin\gamma sin 2\delta \right)^2, \tag{6}$$

$$T_{(22.5,112.5)} = \frac{1}{2}\left\{ \frac{\sin^2 \gamma}{\gamma^2}\left(2\alpha^2 + \beta^2 \cos^2 2\delta\right) + \cos^2 \gamma \sin^2 2\delta + \frac{\beta}{\gamma}\sin 2\gamma \sin 4\delta \right\} \tag{7}$$

In order to obtain a better accuracy, in the values of $\beta(V)$ and $\delta(V)$ we made measurements for these three experimental configurations at four different wavelengths (633 nm from a He-Ne laser, and 514 nm, 488 nm and 458 nm from an Ar laser). As described in ref. [16] in our fit of the experimental data, we look for the set of values of $\beta(V)$ and $\delta(V)$ that minimizes the square of the difference between the experimental data and the theoretically calculated values. In addition, we used the wavelength dependence of the off state birefringence to scale the values of $\beta(V)$ and $\delta(V)$ for the different wavelengths. Our experimental ratios are 1.3, 1.4 and 1.56 respectively for the 514 nm, 488 nm and 458 nm wavelengths compared with the 633 nm wavelength.

The experiments were conducted with the brightness and contrast controls of the videoprojector at 50 and 100 respectively. The maximum value of these controls is 100. We have measured the intensity at intervals of every 10 gray levels. The gray level we send to the display is a magnitude that is related with the voltage. For the Sony VPL-V500 videoprojector electronics, the voltage decreases monotonically when the gray level increases. We have found that an increase in the brightness produces a decrease in the voltage offset, and an increase in the contrast produces an increase in the absolute value of the voltage gain. As the magnitude we control is the gray level sent by the frame-grabber, the values of β and δ are given as a function of the gray level. Figure 2 shows the results obtained for β and δ as a function of the gray level addressed to the LCD. They correspond to the wavelength 458 nm. The maximum value of β is 231 degrees and the maximum value of δ is 25 degrees.

4.- Search for a desired modulation configuration

Once the values of $\beta(V)$ and $\delta(V)$ have been obtained it is possible to make a search for a desired modulation behavior by changing the external polarization system. We use the most general architecture to generate and detect elliptically polarized light by considering that the waveplates introduce arbitrary retardance and by allowing that the angles between the slow axis of the waveplates and the director axis at the input and at the output faces of the SLM can take any value. In this way we have more degrees of freedom to look for a desired amplitude or phase modulation.

The experimental scheme we use in this work is presented in figure 3. A wave-plate introducing a retardance $2\phi_1$ is placed between the first polarizer and the LCD. A second wave-plate introducing a retardance $2\phi_2$ is placed between the LCD and the second polarizer. The angles of the elements in front of the LCD are referred to the orientation of the LC director at the input surface (which we suppose that coincides with the *x*-coordinate axis). The angle φ_1 denotes the orientation of the transmission axis of the first polarizer and the angle η_1 denotes the orientation of the slow axis of the first wave-plate. On the other hand the angles φ_2 and η_2 correspond to the orientation of the transmission axis of the second polarizer and the slow axis of the second wave-plate. For these two last elements the angles are measured with respect to the orientation of the LC director at the output surface (i.e., rotated an angle α with respect to the *x*-coordinate axis).

The Jones vector E_{OUT} at the end of the optical system may be obtained by the following Jones matrix calculation

$$E_{OUT} = P_0 \cdot R(\alpha+\varphi_2)\cdot R(-\alpha-\eta_2)\cdot W(2\phi_2)\cdot R(\alpha+\eta_2) \cdot M_{LCD}(\alpha,\beta,\delta)\cdot R(-\eta_1)\cdot W(2\phi_1)\cdot R(\eta_1)\cdot \begin{bmatrix} cos\varphi_1 \\ sin\varphi_1 \end{bmatrix}. \quad (8)$$

where P_0 represents the matrix of a linear polarizer oriented parallel to the x-coordinate axis, i.e.,

$$P_0 = \begin{bmatrix} 1 & 0 \\ 0 & 0 \end{bmatrix}. \tag{9}$$

and W(2ϕ) is the matrix of a wave-plate centered on the coordinate axis, i. e.,

$$W(2\phi) = \begin{bmatrix} exp(-i\phi) & 0 \\ 0 & exp(+i\phi) \end{bmatrix}. \tag{10}$$

The complex amplitude transmittance, E_t, for this system can be obtained by Jones calculation and the result is given by

$$E_t = exp(-i(\beta + 2\delta))(A_{RE} + iA_{IM}) \tag{11}$$

where A_{RE} and A_{IM} are real magnitudes whose expressions are

$$\begin{aligned} A_{RE} = {} & X[cos f_1 \, cos f_2 \, cos(j_1 - j_2) - sin f_1 sin f_2 \, cos(2(h_1 - h_2) - j_1 + j_2)] \\ & + Y[-cos f_1 sin f_2 \, cos(2h_2 + j_1 - j_2) - sin f_1 \, cos f_2 \, cos(2h_1 - j_1 + j_2)] \\ & + Z[cos f_1 \, cos f_2 sin(j_1 - j_2) - sin f_1 sin f_2 sin(2(h_1 - h_2) - j_1 + j_2)] \end{aligned} \tag{12a}$$

$$\begin{aligned} A_{IM} = {} & X[-cos f_1 sin f_2 \, cos(2h_2 - j_1 - j_2) - sin f_1 \, cos f_2 \, cos(2h_1 - j_1 - j_2)] \\ & + Y[-cos f_1 \, cos f_2 \, cos(j_1 + j_2) + sin f_1 sin f_2 \, cos(2(h_1 + h_2) - j_1 - j_2)] \\ & + Z[cos f_1 sin f_2 sin(2h_2 - j_1 - j_2) - sin f_1 \, cos f_2 sin(2h_1 - j_1 - j_2)] \end{aligned} \tag{12b}$$

Then the intensity transmittance, T, for this system is obtained as

$$T = A_{RE}^2 + A_{IM}^2 \tag{13}$$

and the phase shift is given by

$$\psi = -\beta - 2\delta + atan\left(\frac{A_{IM}}{A_{RE}}\right) \tag{14}$$

As β(V) and δ(V) have already been measured, it is possible to perform a computer search for a desired modulation. In the optimization process we assign initial arbitrary values to the angles η_1, η_2, φ_1 and φ_2, then the transmittance T and the phase-shift ψ can be calculated using equations (13) and (14). The optimization criterion to be applied depends on the complex transmittance modulation we are interested on.

In case two variable wave-plates are available (for instance using Soleil-Babinet compensators), the computation of the search for a desired modulation may also include ϕ_1 and ϕ_2 as free parameters. In any other case the values of ϕ_1 and ϕ_2 are fixed by the available wave-plates. In our case the retardance of the available wave-plates are $2\phi_1$ = 125 degrees and $2\phi_2$ = 94.5 degrees for the wavelength 458 nm. Also the cases $2\phi_1 = 2\phi_2 = 0$ have been considered, corresponding to the situation when no wave-plates are present. We have used the dichroic polymer (DP) polarizers with the coating Vis-1 designed for the visible, fabricated by Meadowlark Optics. The wave-plates we use are multiple order quarter wavelength wave-plates made by Tower Optical Corporation. The one at the input of the LCD is for the 633 nm wavelenth and the one at the output is for the 488 nm. Their retardances at 458 nm were measured by a procedure that can be found in [23].

(a) Phase-only modulation

Phase-only modulation is desirable for a wide set of optical elements. The optimal modulation consists in a flat amplitude modulation and a phase modulation varying from 0 to 2π radians. It has been demonstrated that good phase mostly modulation can be obtained with thick LCDs operating between linear polarizers [24,25]. However, it is difficult to obtain it with thinner displays.

We search for the set of values η_1, η_2, φ_1 and φ_2 that minimizes the difference $T_{\max} - T_{\min}$ over the entire voltage range. $T_{\max}$ and $T_{\min}$ represent the maximum and the minimum values of the intensity transmitted by the display (eq. (13)). The transmittance may not be maximal, but we are interested in a configuration where it remains constant. First we consider the situation when no wave-plates are present. The result of the optimization search leads to the following angles: $\varphi_1 = 22$ degrees and $\varphi_2 = -21$ degrees. Figure 4(a) shows the intensity and phase modulations obtained with this configuration. The symbols correspond to the experimentally measured data and the continuous lines to the corresponding theoretical data. The agreement between the experimental measurements and the numerical values is excellent for both intensity

and phase modulation. The predicted variation in intensity transmission is 49% from the maximum to the minimum value, and the phase depth is 1.5π radians.

The second situation we consider is using the two wave-plates previously described with phase-shifts $2\phi_1 = 125$ degrees and $2\phi_2 = 94.5$ degrees. The result of the computation for a flat intensity transmission leads to the angles $\varphi_1 = 26$, $\eta_1 = 0$, $\varphi_2 = -16$ and $\eta_2 = 11$ degrees. Figure 4(b) shows the intensity and phase transmissions obtained with this configuration. Again the agreement between the experimental and the theoretical values is excellent. The predicted intensity modulation is almost flat, having a variation of 4 % over the entire range of gray levels. The predicted phase depth is 2π radians.

One can see that by using waveplates it is possible to obtain a better phase only configuration: the intensity variations are very small and the obtained phase depth for 458 nm is 2π radians.

(b) Amplitude-only modulation

Amplitude-only modulation is another configuration desirable in optical image processors to implement the input image. In this configuration we seek for the position of the polarization elements that leads to a flat phase response and a maximum intensity contrast (ratio $T_{\max}/T_{\min}$), while keeping a monotonic intensity transmittance response with the gray level. The optimization criterion we use is a trade off between these three conditions. Again we consider the situation with and without wave-plates.

For the case of linear polarizers only (no waveplates are introduced), the optimization search leads to the polarizer transmission axis angles $\varphi_1 = 91$ and $\varphi_2 = 89$ degrees. Note that this means that the transmission axis of both polarizers are perpendicular to the director axis at the input face and at the output face respectively. The optimization search leads us to the configuration that has been usually considered in the literature as the optimum one for amplitude-only modulation. Figure 5(a) shows the intensity and phase transmissions obtained

with this configuration. The predicted contrast is 198:1 and the phase depth is 0.65π radians. If the wave-plates are used ($2\phi_1 = 125$ and $2\phi_2 = 94.5$ degrees) the optimization leads to the angles $\varphi_1 = 116$, $\eta_1 = 96$, $\varphi_2 = 62$ and $\eta_2 = -7$ degrees. Figure 5(b) shows the intensity and phase transmissions obtained with this configuration. The predicted contrast is 100:1. The amplitude-only modulation has been greatly improved with respect to the case with no wave-plates because now the phase depth is as low as 0.18π radians and we obtain an almost linear behavior of the transmitted intensity in the gray level range.

We can see in these figures the excellent agreement obtained between the predicted and the measured results. The use of the waveplates improves the modulation characteristics with respect to the case when we only use linear polarizers. We have obtained almost a linear intensity modulation with a very small phase modulation.

Both in the phase-only modulation configuration and in the amplitude-only modulation configuration we have obtained an excellent agreement between prediction and experiment. The slight differences that appear can be explained because of the interference and diffraction and interference effects shown by Davis et al [26].

5.- Conclusions

A method to predict the optimum polarization configuration that leads to a desired modulation behavior of the LCD has been demonstrated. This method is based on a model of the LCD which takes into account the existing edge effects. Through this model we characterize the Jones matrix of the LCD in terms of two voltage dependent magnitudes $\beta(V)$ and $\delta(V)$. Once the device has been characterized a computational search for a desired modulation is performed. We have looked for polarization configurations leading to a phase-only modulation and an amplitude-only modulation, which are interesting configurations in an optical processor. A generalised architecture to generate and detect elliptically polarized light has been proposed. It has been shown that adding wave-plates to the optical setup (before and behind the LCD) greatly improves the modulation capabilities of the LCD. An excellent agreement between the

predicted complex transmittance and the experimentally measured validates the potentiality of the method proposed.

Acknowledgements

This work has been financed by Dirección General de Enseñanza Superior del Ministerio de Educación y Cultura de from Spain, project number PB96-1134-C02-01. A. Márquez thanks the Comissionat per a Universitats i Recerca de la Generalitat de Catalunya for a grant.

References

[1] H. K. Liu, J. A. Davis and R. A. Lilly, "Optical-data-processing properties of a liquid crystal television spatial light modulator," *Optics Letters* **10**, 635-637 (1985)

[2] H.-K. Liu and T.-H. Chao, "Liquid crystal television spatial light modulators," *Applied Optics* **28**, 4772-4780 (1989)

[3] J. L. De Bougrenet de Tocnaye and L. Dupont, "Complex amplitude modulation by use of liquid-crystal spatial light modulators," *Applied Optics* **36**, 1730-1741 (1997)

[4] V. Laude and Ph. Réfregier, "Multicriteria characterization of coding domains with optimal Fourier spatial light modulators filters," *Applied Optics* **33**, 4465-4471 (1994)

[5] R. D. Juday, J. L. Lacroix, and P. Karivaratha Rajan, "Selection of LCTV operating curves for input and filter", in Optical Pattern Recognition III, D. P. Casasent and T. H. Chao, eds., Proc. SPIE, **1701**, 78-82 (1992)

[6] D. W. Berreman, "Optics in smoothly varying anisotropic planar structures: Application to liquid-crystal twist cells," *J. Opt. Soc. Am.* **63**, 1374-1380 (1973)

[7] D. W. Berreman, "Dynamics of liquid-crystal twist cells," *Applied Physics Letters*, **25**, 12-15 (1974)

[8] D. B. Taber, J. A. Davis, L. A. Holloway, Jr. , and O. Almagor, "Optically controlled Fabry-Perot interferometer using a liquid crystal light valve," *Applied Optics* **29**, 2623-2631 (1990)

[9] C. Z. van Doorn, "Dynamic behavior of twisted nematic liquid-crystal layers in switched fields," *Journal of Applied Physics* **46**, 3738-3745 (1975)

[10] C.-J. Chen, A. Lien and M. I. Nathan, "Simple method for the calculation of the deformation profiles in chiral liquid crystal cells with asymmetric pretilt," *Journal of Applied Physics* **81**, 70-73 (1997)

[11] J. C. Kirsch, D. A. Gregory, M. W. Thie and B. K. Jones, "Modulation characteristics of the Epson liquid crystal television," *Optical Engineering* **31**, 963-970 (1992)

[12] L. Gonçalves Neto, D. Roberge and Y. Sheng, "Programmable optical phase-mostly holograms with coupled-mode modulation liquid crystal television," *Applied Optics* **34** (11) 1944-1950 (1995)

[13] K. Lu and B. E. A. Saleh, "Theory and design of the liquid crystal TV as an optical spatial phase modulator," *Optical Engineering* **29**, 240-246 (1990)

[14] M. Yamauchi and T. Eiju, "Optimization of twisted nematic liquid crystal panels for spatial light phase modulation," *Optics Communications* **115**, 19-25 (1995)

[15] J. A. Coy, M. Zaldarriaga, D. F. Grosz and O. E. Martínez, "Characterization of a liquid crystal television as a programmable spatial light modulator," *Optical Engineering*, **35**, 15-19 (1996)

[16] A. Márquez, J. Campos, M. J. Yzuel, I. Moreno, J. A. Davis, C. Iemmi, A. Moreno and A. Robert, "Characterization of edge effects in twisted nematic liquid crystal displays," Opt. Eng. **39**, 3301-3307 (2000)

[17] J. A. Davis, I. Moreno and P. Tsai, "Polarization eigenstates for twisted-nematic liquid crystal displays," *Applied Optics*, **37**, 937-945 (1998)

[18] J. L. Pezzanitti and R. A. Chipman, "Phase-only modulation of a twisted nematic liquid-crystal TV by use of the eigenpolarization states," *Optics Letters* **18** (18), 1567-1567 (1993)

[19] I. Moreno, J. A. Davis, K. G. D'Nelly y D. B. Allison, "Transmission and phase measurements for polarization eigenvectors in twisted-nematic liquid-crystal spatial light modulators", *Optical Engineering* **37**, 3048 (1998)

[20] C. Soutar y K. Lu, "Determination of the physical properties of an arbitrary twisted-nematic liquid crystal cell," *Optical Engineering* **33**, 2704-2712 (1994)

[21] J. A. Davis, D. B. Allison, K. G. D'Nelly, M. L. Wilson and I. Moreno, "Ambiguities in measuring the physical parameters for twisted-nematic liquid crystal spatial light modulators," *Optical Engineering*, **38**, 705-709 (1999)

[22] J. A. Davis, P. Tsai, K. G. D'Nelly y I. Moreno, “Simple technique for determining the extraordinary axis direction for twisted nematic liquid crystal spatial light modulators,” *Optical Engineering*, **38**, 929-932 (1999)

[23] M. Born and E. Wolf, Principles of optics, 7th edition, Section 15.4.3, Cambridge University Press, (1999).

[24] N. Konforti, E. Marom and S.-T. Wu, “Phase-only modulation with twisted nematic liquid-crystal spatial light modulators,” *Optics Letters* **28** (3), 4845-4852 (1989)

[25] T. H. Barnes, T. Eiju, K. Matsuda and N. Ooyama, “Phase-only modulation using a twisted nematic liquid crystal television,” *Applied Optics* **28** (22) 4845-4852 (1989)

[26] J. A. Davis, P. Tsai, D. M. Cottrell, T. Sonehara, and J. Amako, “Transmission variations in liquid crystal spatial light modulators caused by interference and diffraction effects”, Opt. Eng., **38**, 1051-1057, (1999)

Figure captions

Figure 1.

Model of the LCD with edge layers that do not tilt. (a) Twist angle as a function of LCD depth. (b) Difference of refraction index as a function of LCD thickness.

Figure 2

Measured parameters as a function of gray level for wavelength 458nm. (a) Values of $\beta(V)$, (b) values of $\delta(V)$.

Figure 3

Arrangement of the polarizing elements in the set-up.

Figure 4

Phase-only modulation. Intensity transmission (■) and phase modulation (♦) measured experimentally. The continuous lines correspond to the theoretical values. Optimal configurations obtained with (a) only polarizers at angles $\varphi_1 = 22$ and $\varphi_2 = -21$ degrees, (b) polarizers and waveplates at angles $\varphi_1 = 26$, $\eta_1 = 0$, $\varphi_2 = -16$ and $\eta_2 = 11$ degrees.

Figure 5

Amplitude-only modulation. Intensity transmission (■) and phase modulation (♦) measured experimentally. The continuous lines correspond to the theoretical values. Optimal configurations obtained with (a) only polarizers at angles $\varphi_1 = 91$ and $\varphi_2 = 89$ degrees, (b) polarizers and waveplates at angles $\varphi_1 = 116$, $\eta_1 = 96$, $\varphi_2 = 62$ and $\eta_2 = -7$ degrees.

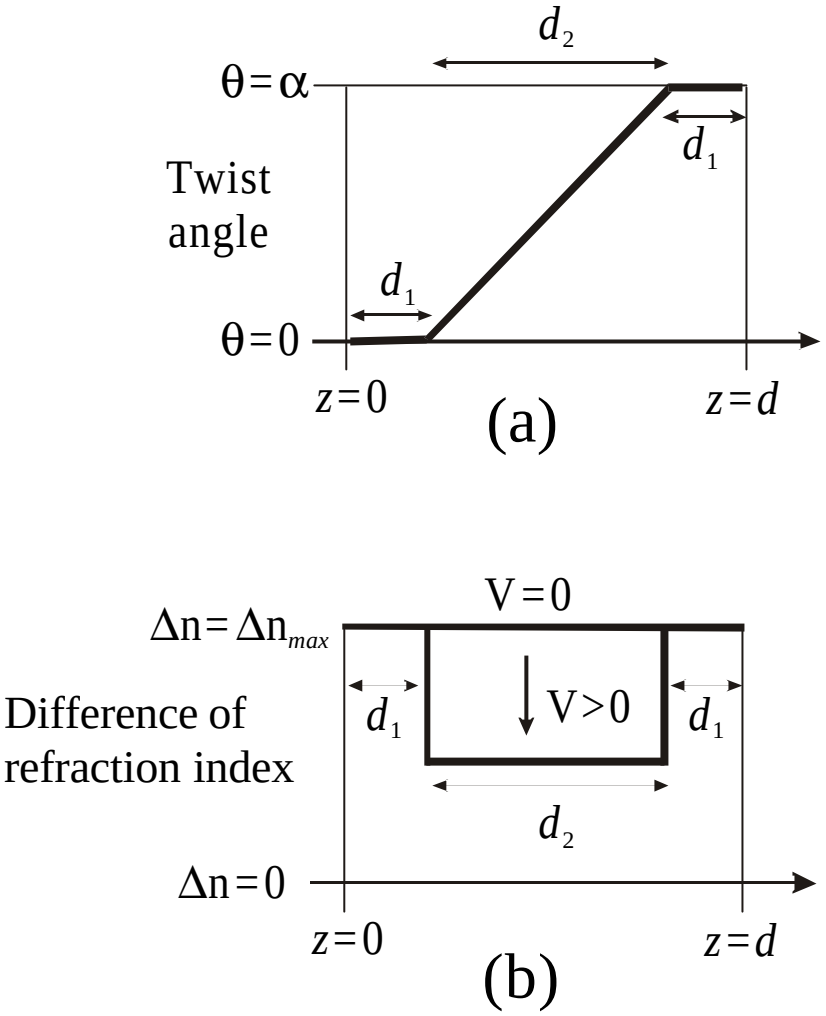

Figure 1.

"Quantitative prediction of the modulation behavior of twisted nematic liquid crystal displays"

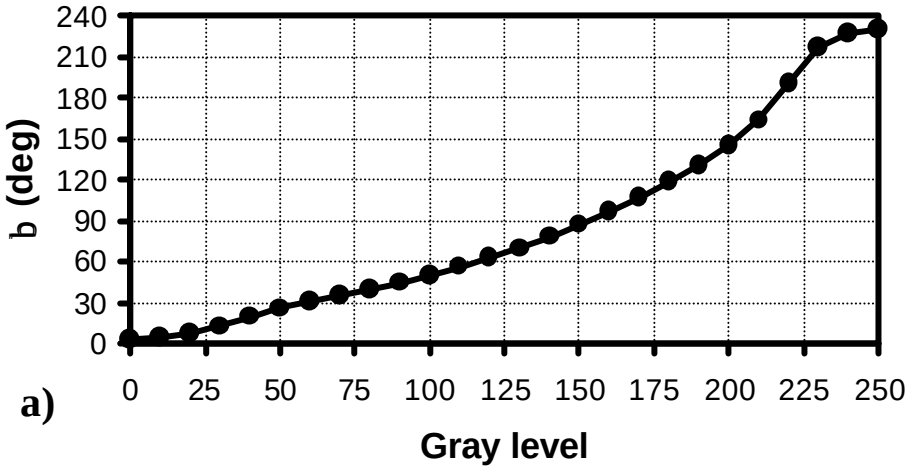

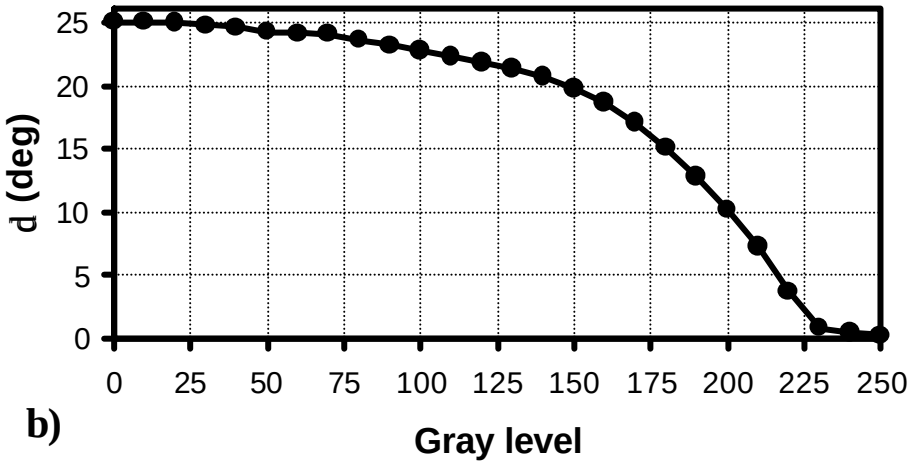

Figure 2.

"Quantitative prediction of the modulation behavior of twisted nematic liquid crystal displays"

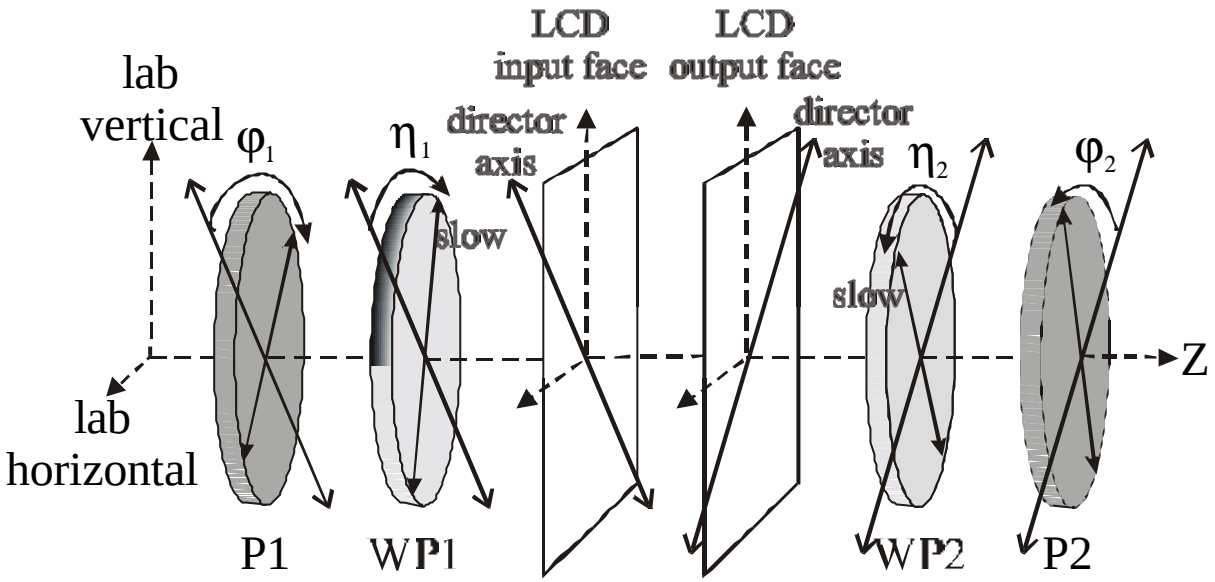

Figure 3

"Quantitative prediction of the modulation behavior of twisted nematic liquid crystal displays"

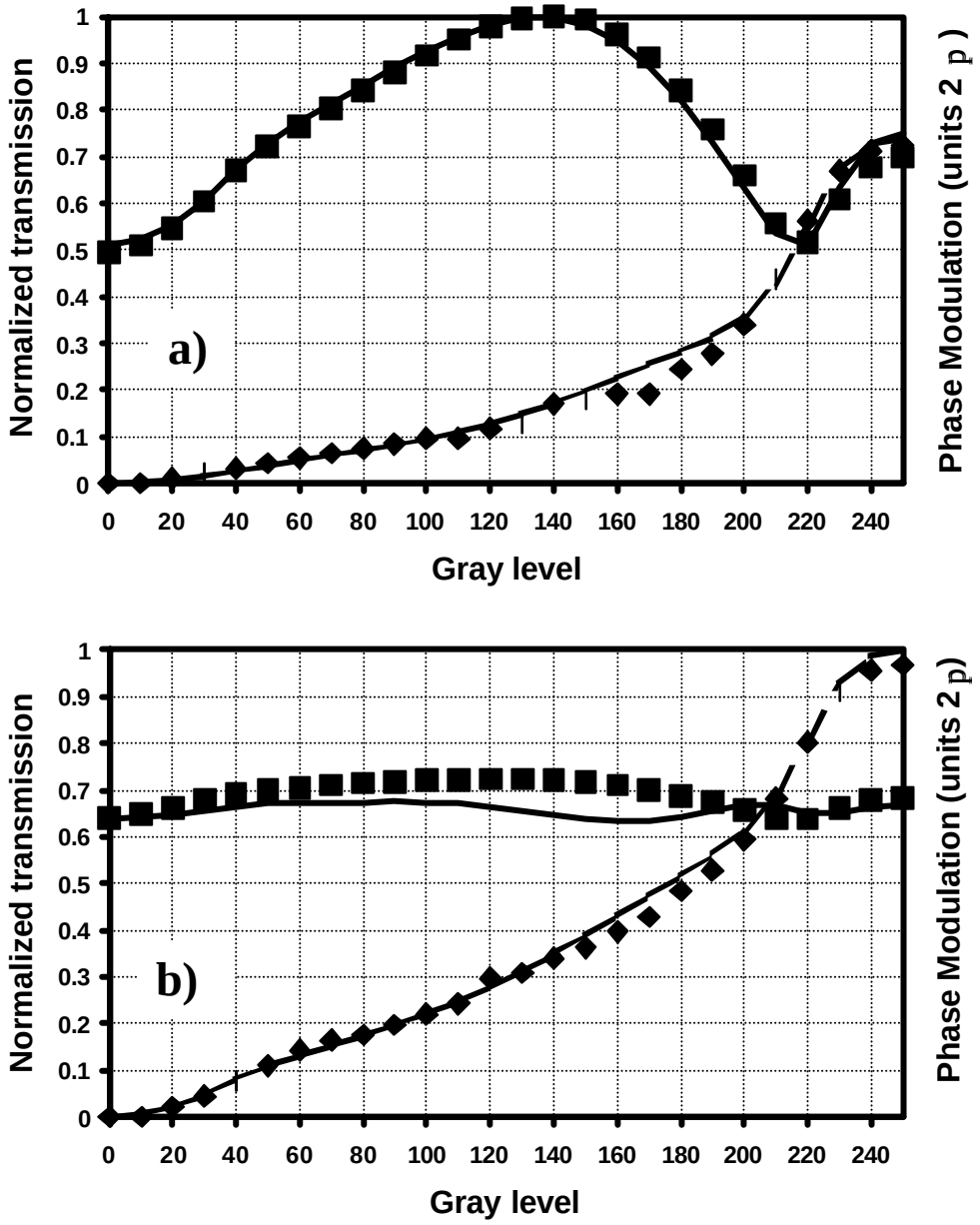

Figure 4

"Quantitative prediction of the modulation behavior of twisted nematic liquid crystal displays"

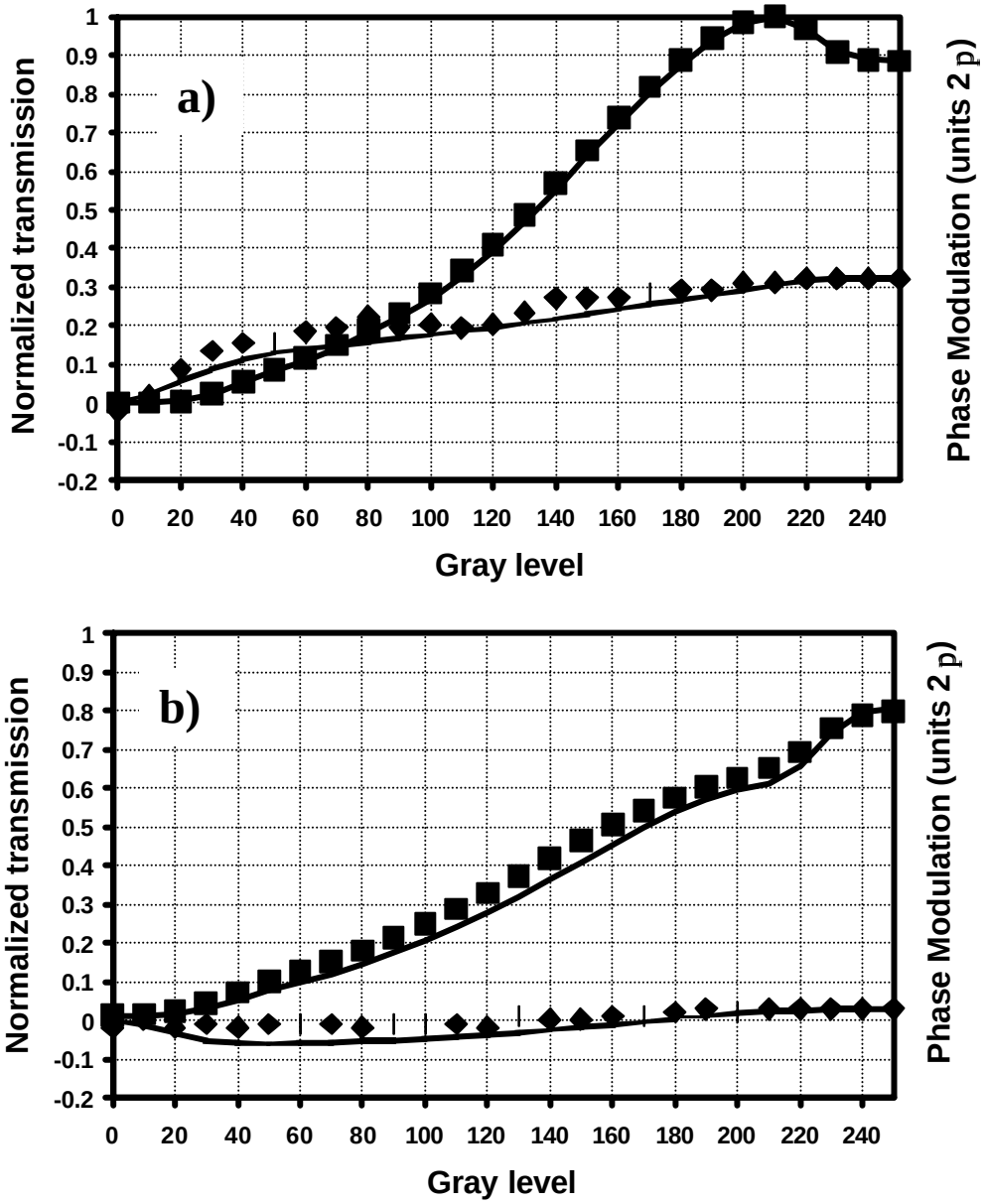

Figure 5

"Quantitative prediction of the modulation behavior of twisted nematic liquid crystal displays"

Programmable axial apodizing and hyperresolving amplitude filters with a liquid-crystal spatial light modulator

Jeffrey A. Davis

Department of Physics, San Diego State University, San Diego, California 92182

Juan Carlos Escalera, Juan Campos, Andres Marquez, and Maria J. Yzuel

Departamento de Fisica, Universidad Autonoma de Barcelona, 08193 Bellaterra, Spain

Claudio Iemmi

Departamento de Fisica, Facultad de Ciencias Exactas y Naturales, Universidad de Buenos Aires, (1428) Buenos Aires, Argentina

Received January 26, 1999

Amplitude-transmitting filters for apodizing and hyperresolving applications can be easily implemented by use of a two-dimensional programmable liquid-crystal spatial light modulator operating in a transmission-only mode. Experimental results are in excellent agreement with theoretical predictions. This approach can permit the analysis of various filter designs and can allow the filters to be changed rapidly to modify the response of an optical system. © 1999 Optical Society of America

OCIS codes: 230.6120, 110.3000.

We demonstrate that amplitude-transmitting filters for apodizing and hyperresolving applications can easily be implemented with a two-dimensional programmable liquid-crystal spatial light modulator (LCSLM) operating in a transmission-only mode. Experimental results are in excellent agreement with theoretical predictions. This approach can permit the analysis of various filter designs and allow the filters to be changed rapidly to modify the response of an optical system.

Nonuniform amplitude transmission filters can be used to modify the response of optical systems.[1–3] Different filter designs can produce apodization or hyperresolution either in the transverse plane[2,3] or along the axis.[3,4] Here we concentrate on filters of the form $t(r) = a + br^2 + cr^4 + dr^6$. These filters were described previously.[4–6] By changing the values of the coefficients one can generate either transverse or axial apodizing filters.

First we consider an aberration-free system that has a system aperture with a normalized radius $r = 1$, as shown by line a in Fig. 1. For this case, the intensity oscillates according to the sinc-squared function shown by curve a in Fig. 2 as the axial position is changed.

The depth of focus (DOF) of the optical system can be increased and the oscillations in intensity in the axial direction can be decreased by use of an axial apodizing filter. Curve b of Fig. 1 shows an example[5] of such an amplitude-transmitting filter given by $t(r) = 6.75r^2 - 13.5r^4 + 6.75r^6$. The theoretically calculated intensity along the axis in curve b of Fig. 2 shows that the depth of focus increases and the oscillatory changes in the intensity are smoothed out.

The DOF can also be decreased by use of an axial hyperresolving filter function such as $t(r) = 1 - 4r^2 + 4r^4$, as shown by curve c of Fig. 1. This filter not only decreases the DOF but also increases the intensity of the secondary maxima in the axial direction,[5] as shown by curve c of Fig. 2. Therefore we consider these axial hyperresolving filters as multifocal filters.

In Fig. 2 the three curves are normalized. The relative intensity values in the peak for the axial apodizing filter and the axial hyperresolving filter are 0.316 and 0.11, respectively. The drawback in using amplitude filters is that the light in the image plane is reduced.

Amplitude pupil filters have been made with photographic emulsions by different techniques.[6,7] However, these pupil functions can be difficult and expensive to fabricate accurately and cannot be changed quickly. Here we show how to program various transmissive filters by using a programmable liquid-crystal display that operates in an amplitude-only mode.

The experimental system is simple. Light from a He–Ne laser with a wavelength of 0.6328 μm is expanded, collimated, and sent through an aperture. It is then passed through a twisted nematic LCSLM panel (Sony Model LCX012BL) for the red channel extracted from a Sony Model VPL-V500 video projector. This device has 640 × 480 pixels, with a pixel spacing of

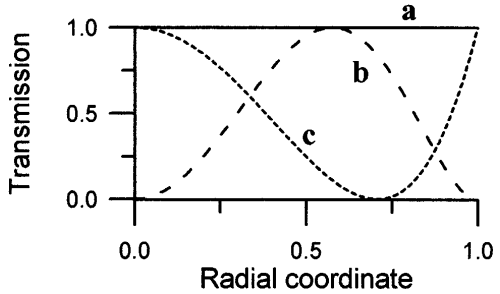

Fig. 1. Amplitude pupil filter functions corresponding to a, uniform transmission; b, an axial apodizing filter, where $t(r) = 6.75r^2 - 13.5r^4 + 6.75r^6$; c, an axial hyperresolving filter, where $t(r) = 1 - 4r^2 + 4r^4$.

0146-9592/99/090628-03$15.00/0

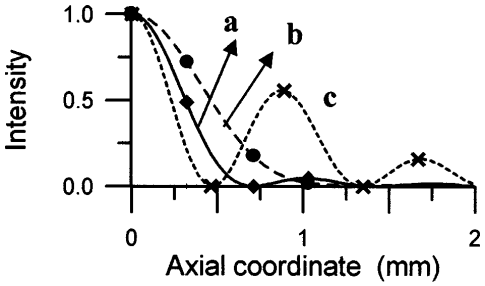

Fig. 2. Theoretically calculated intensity as a function of axial distance for the filters of Fig. 1. Symbols show axial positions where experimental measurements were made: a, uniform transmission; b, an axial apodizing filter, where $t(r) = 6.75r^2 - 13.5r^4 + 6.75r^6$; c, an axial hyperresolving filter, where $t(r) = 1 - 4r^2 + 4r^4$.

41 μm and a window size of 34 μm. The aperture that we use has a diameter of approximately 400 pixels.

The light passing through the LCSLM is focused with a 20-cm focal-length lens. The focused spot is magnified with a 40× microscope objective and imaged onto a CCD camera. The microscope objective also serves as a spatial filter to eliminate higher-order diffracted images caused by the pixel structure of the LCSLM. To examine various defocus planes, we fix the distance between the microscope objective and detector and translate the entire objective–detector system.

The operating parameters of the liquid-crystal display (twist, birefringence, and orientation of director axis) were measured by various techniques.[8–10] For our device, the twist angle is −96.3 deg, the birefringence is 155.8 deg, and the extraordinary birefringence axis is oriented at 47.2 deg relative to the vertical directions. Most researchers who use these devices are interested in either a coupled amplitude and phase modulation or a phase-only modulation. In our case, we want amplitude modulation without any phase modulation. To eliminate phase modulation[11] we polarize the input light perpendicular to the director axis at the input side (the direction of the ordinary index of refraction), and the output polarizer is perpendicular to the director axis at the output side (which is also the direction of the ordinary index of refraction). In this configuration, there is no phase modulation.

One controls the transmission for the panel by sending a voltage signal to each pixel of the display from a video card in a computer. This video card sends gray-level signals that have values from 0 to 256. The transmitted intensity is monitored as a function of gray level to calibrate the display. Using these results, we formulate a calibration look-up table of amplitude transmittance (t) versus gray level (g).

As we discussed above, the numerically calculated intensity distributions for the clear aperture and for the two filters are as shown in Fig. 2. These numerical results predict that the axial apodizing filter of Fig. 1, curve b, will increase the DOF and that the axial hyperresolving filter shown in curve c of Fig. 1 will produce multifocal behavior and decrease the DOF. For Fig. 2, the axial coordinate scale was calculated with our experimental parameters.

Figure 3(a) shows the experimental results obtained with a clear aperture. Each three-dimensional (3-D) plot shows the intensity distribution in a different axial plane (these planes coincide with those that are marked in Fig. 2). The sinc-squared behavior of the focused spot intensity is clearly shown. Fortunately, the focused images show no effects of aberrations caused by the LCSLM panel.

Figure 3(b) shows the experimental results for the axial apodizing filter design shown as curve b of Fig. 1. Again, each 3-D plot shows the intensity distribution in a different axial plane. We see that the intensity in the center of the plots decreases more slowly than in the clear aperture [Fig. 3(a)]. Experimental results are in excellent agreement with the theoretical predictions of Fig. 2, curve b.

Figure 4 shows the results for the axial hyperresolving filter of Fig. 1, curve c. In this case the axial intensity diminishes and then increases to form sequential focuses at different axial distances. Figure 4(a) shows the 3-D plots of the intensities, and Fig. 4(b) shows the two-dimensional intensity distributions at several axial positions. Again the positions

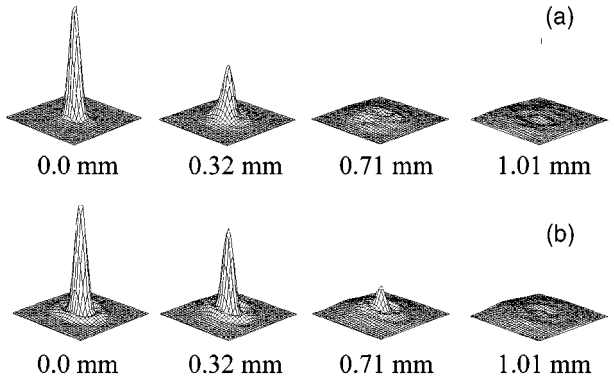

Fig. 3. Experimental measurements of the intensity of the focused spot at the axial positions denoted in Fig. 2: (a) with the uniformly transmitting filter of Fig. 1, line a, the intensity changes according to the expected sinc-squared behavior. (b) with the axial apodizing filter of Fig. 1, curve b, the intensity decreases more slowly as a function of axial distance, showing that the DOF has been increased.

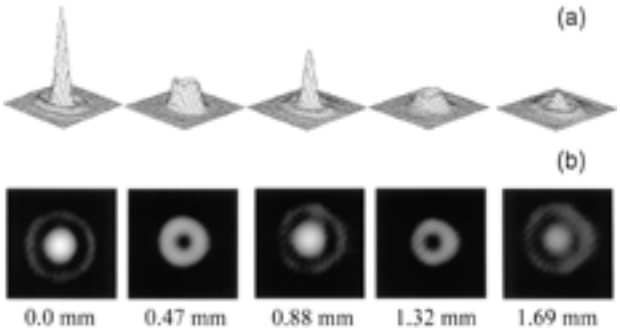

Fig. 4. Experimental measurements of the intensity of the focused spot at the axial positions denoted in Fig. 2 with the axial hyperresolving filter of Fig. 1, curve c. The intensity oscillates with axial position, as predicted by theory: (a) 3-D plots at various axial positions; (b) two-dimensional intensity plots at various axial positions.

of these planes are shown in Fig. 2. The gray levels of Fig. 4(b) have been saturated to show the secondary maxima about the principal maximum. The multifocal behavior of this filter is clearly shown: The intensity drops to zero before increasing to a second and third focus. These results are in excellent agreement with the theory shown in curve c of Fig. 2.

In conclusion, we report the use of an amplitude-transmitting LCSLM to introduce programmable apodizing filters into optical systems. Experimental results for axial apodizing and hyperresolving filters are in excellent agreement with theoretical predictions. The technique is easy to implement and should allow experimental results for various transmissive filters to be obtained easily.

This research was partially financed by the Direccion General de Ensenanza Superior del Ministerio de Educacion y Cultura under project PB96-1134-C02-01 and the "Programa de Cooperacion Cientifica con Iberoamerica" (Spain). J. A. Davis gratefully acknowledges the financial support of the Direccion General de Investigacion Cientifica y Tecnica, Ministerio de Education y Cultura (Spain). C. Iemmi gratefully acknowledges the support of the Universidad de Buenos Aires, Consejo Nacional de Investigaciones Cientificas y Tecnicas and Fundacion Antorchas (Argentina). A. Marquez thanks the Comissionat per a Universitats i Recerca de la Generalitat de Catalunya (Spain) for a grant. J. Campos's e-mail address is ifop8@cc.uab.es.

References

1. J. P. Mills and B. J. Thompson, J. Opt. Soc. Am. **3,** 694 (1986).
2. C. S. Chung and H. H. Hopkins, J. Mod. Opt. **35,** 1485 (1988).
3. J. Campos and M. J. Yzuel, J. Mod. Opt. **36,** 733 (1989).
4. M. J. Yzuel, J. C. Escalera, and J. Campos, Appl. Opt. **29,** 1631 (1990).
5. R. Hild, J. C. Escalera, M. J. Yzuel, and R. Muschall, Pure Appl. Opt. **14,** 795 (1995).
6. C. J. R. Sheppard and Z. S. Hegedus, J. Opt. Soc. Am. A **5,** 643 (1988).
7. E. W. S. Hee, Opt. Laser Technol. **4,** 75 (1975).
8. C. Soutar and K. Lu, Opt. Eng. **33,** 2704 (1994).
9. J. A. Davis, D. B. Allison, K. G. D'Nelly, M. L. Wilson, and I. Moreno, "Ambiguities in measuring the physical parameters for liquid crystal spatial light modulators," Opt. Eng. (to be published).
10. J. A. Davis, P. Tsai, K. G. D'Nelly, and I. Moreno, "Simple technique for determining the extraordinary axis direction for twisted nematic liquid crystal spatial light modulators," Opt. Eng. (to be published).
11. K. Lu and B. E. A. Saleh, Opt. Eng. **29,** 240 (1990).

Inherent apodization of lenses encoded on liquid-crystal spatial light modulators

María J. Yzuel, Juan Campos, Andrés Márquez, Juan C. Escalera, Jeffrey A. Davis, Claudio Iemmi, and Silvia Ledesma

Focusing diffractive optical elements encoded in liquid-crystal spatial light modulators yields an inherent equivalent apodization of the focused spot as a result of the pixelated nature of these devices and the finite extent of each pixel. We present a theoretical explanation for and experimental evidence of this effect. We demonstrate an experimental procedure for measuring the apodization and a method to compensate for this effect. © 2000 Optical Society of America

OCIS codes: 230.3720, 120.4820, 110.4100, 110.2990, 260.1960.

1. Introduction

Diffractive optical elements (DOE's) are playing an increasingly prominent role in a variety of applications, including focusing lenses and both optical and digital holography.[1] At the same time, advances in the technology of spatial light modulators (SLM's) permit the implementation of DOE's whose characteristics can be changed dynamically.[2–4]

Davis *et al*. reported[2] that binary Fresnel phase-encoded lenses can be encoded on a programmable SLM. Cottrell *et al*. have shown[3] that Fresnel phase-encoded lenses can produce multiple spots when the focal length decreases. Carcolé *et al*.[5] studied a mathematical model to describe the behavior of low-resolution Fresnel lenses encoded on SLM's.

Many of the effects reported in Refs. 3–5 are caused by the sampling of the quadratic phase imposed by the pixelated structure of the SLM. The sampling causes the appearance of multiple lenses when the sampling frequency is lower than the Nyquist frequency.

M. J. Yzuel, J. Campos (e-mail: juan.campos@uab.es), A. Márquez, and J. C. Escalera are with the Departamento de Física, Universidad Autónoma de Barcelona, 08193 Bellaterra, Spain; J. A. Davis is with the Department of Physics, San Diego State University, San Diego, California 92182; and C. Iemmi and S. Ledesma are with the Departamento de Física, Facultad de Ciencias Exactas y Naturales, Universidad de Buenos Aires, 1428 Buenos Aires, Argentina.

Received 24 August 1999; revised manuscript received 2 August 2000.

0003-6935/00/326034-06$15.00/0

However, Carcolé *et al*.[5] demonstrated that the image produced by a lens encoded onto a SLM appears to be convolved with a rectangle function that corresponds to the pixel shape. This effect leads to apodization[5,6] of the image produced by the lens and is the subject of this paper. This effect is particularly important not only for lenses encoded onto SLM's but also for all focusing DOE's. In this paper we discuss the theoretical explanation for this apodizing effect. We show experimental measurements of the apodizing effect and demonstrate an experimental method that allows us to compensate for it by introducing an equivalent pupil that has a nonuniform transmission. We combine the focusing properties of the DOE and the amplitude transmission function onto a single phase-only liquid-crystal spatial light modulator (LCSLM). In Section 2 we briefly discuss the theory of the inherent equivalent apodization. The experimental setup is described in Section 3. The experimental measurement of the inherent equivalent apodization is shown in Subsection 4.A. We demonstrate in Subsection 4.B that this inherent apodization can be compensated for. Finally, the conclusions of the paper are given in Section 5.

2. Theory

We can encode a converging lens in a phase-only SLM by displaying the quadratic phase function $\phi_Q(r)$ as

$$Z^*(u) = \exp[-i\phi_Q(r)] = \exp[-i(\pi u^2/\lambda f)]. \quad (1)$$

Here the focal length is represented by f, and we use one-dimensional notation for simplicity. If we encode this lens on a pixelated device that has a length

L with a pixel spacing of D and a pixel width of W, the transmission of the SLM will be

$$T(u) = \left\{\left[Z^*(u)\sum_n \delta(u - nD)\right]\mathrm{rect}(u/L)\right\} \otimes \mathrm{rect}(u/W), \tag{2}$$

where $\otimes$ represents the convolution operation. Equation (2) means that the operations that we are performing when we encode the quadratic phase function are the following: sampling the function at distances D given by the spacing of the pixels, spatially limiting the function because of the finite extent (L) of the SLM, and convolving this sampled function by the shape of the pixel as a result of the finite width (W) of the pixel. Then across the pixel we will have the same phase value; as we will see in what follows, this is the difference between a continuous refractive lens and a spatially quantized lens.

When the SLM is illuminated by a plane wave,[5] the amplitude distribution in the focal plane of the encoded lens is given by Fresnel diffraction and can be obtained by convolution of Eq. (2) with a quadratic diverging phase function given by $Z(u)$, say

$$U(x) = \int T(u)Z(x - u)\mathrm{d}u. \tag{3}$$

Note that we have to perform two convolutions [Eqs. (2) and (3)]. By using the associative and commutative properties of the convolution function, we can write the amplitude in the focal plane as

$$U(x) = \left\{\int \left[Z^*(u)\sum_n \delta(u - nD)\right]\mathrm{rect} \times Z(x - u)\mathrm{d}u\right\} \otimes \mathrm{rect}\left(\frac{x}{W}\right). \tag{4}$$

We can evaluate the amplitude in the focal plane by first calculating the propagation of the sampled lens (without taking into account the pixel size) and then convolving the result with the pixel shape. Apart from a constant multiplicative factor, the result is given by

$$U(x) = \left\{\exp\left(i\frac{\pi}{\lambda f}x^2\right)\left[\mathrm{sinc}\left(\frac{Lx}{\lambda f}\right) \otimes \sum_n \delta\left(x - n\frac{\lambda f}{D}\right)\right]\right\} \otimes \mathrm{rect}\left(\frac{x}{W}\right), \tag{5}$$

where $\mathrm{sinc}(x) = \sin(\pi x)/(\pi x)$. Equation (5) yields a superposition of sinc functions that have widths of $(\lambda f)/L$ and separations of $(\lambda f)/D$. The separations between the sinc functions are much larger than the widths of the functions because $L = ND$, where N is the number of pixels in a row of the SLM. Because we are interested in evaluating the amplitude in the central zone of the focal plane, we have to consider only the contribution of the $n = 0$ sinc function. In addition, the quadratic phase term in Eq. (5) can be neglected in the central zone because its phase variations across the rectangle function and the central lobe of the sinc function are much less than 2π rad. In this case the amplitude in the focal plane can be written as

$$U(x) = \mathrm{sinc}(Lx/\lambda f) \otimes \mathrm{rect}(x/W). \tag{6}$$

This result shows that the shape of the focused spot will be convolved with a rectangle function that has the width of the pixels in the SLM.

In image formation, the amplitude distribution in the focal plane is equal to the Fourier transform of the pupil function. Consequently, we have an effective pupil function that is equal to the Fourier transform of Eq. (6). This pupil function is given by the product of a rectangle function of width L that corresponds to the size of the SLM and a sinc function that corresponds to the Fourier transform of the pixel. This sinc function acts as a nonuniform transmission pupil $\tau(u)$ that acts as an equivalent apodizing function and is defined as

$$\tau(u) = \mathrm{sinc}(Wu/\lambda f). \tag{7}$$

The effects of this equivalent apodizing function will become more severe as the width of the pixel increases or as the focal length of the lens decreases.

At this point we remark on the difference that exists when no lens is addressed onto the pixelated SLM and the focusing of light is produced by a refractive lens placed just behind the SLM. Then the amplitude of the wave front behind the lens is expressed by

$$T'(u) = \left\{\left[\sum_n \delta(u - nD)\mathrm{rect}(u/L)\right] \otimes \mathrm{rect}(u/W)\right\}Z^*(u). \tag{8}$$

Note that now the phase across the pixel dimension is not constant. As was true for Eq. (3), the amplitude distribution in the focal plane of the lens is given by Fresnel diffraction and can be obtained by convolution of Eq. (8) with a quadratic diverging phase function given by $Z(u)$ [Eq. (1)]. Apart from a constant multiplicative factor, the result is

$$U'(x) = \left\{\exp\left(i\frac{\pi}{\lambda f}x^2\right)\left[\mathrm{sinc}\left(\frac{Lf}{\lambda f}\right) \otimes \sum_n \delta\left(x - n\frac{\lambda f}{D}\right)\right]\right\}\mathrm{sinc}\left(\frac{Wx}{\lambda f}\right), \tag{9}$$

where the effect of the pixel in the amplitude distribution in the focal plane is the product by the $\mathrm{sinc}(Wx/\lambda f)$ function. The effect of the pixel is clearly different in this case from that when a lens is displayed on the SLM [Eqs. (5) and (6)] in which we obtain in the focal plane a convolution operation with the rectangle function that expresses the pixel shape and width. In the case of the encoded lens in the

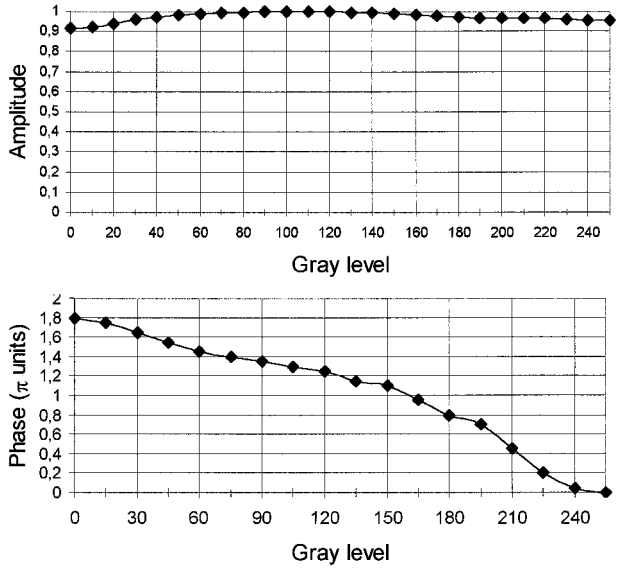

Fig. 1. Normalized amplitude transmission and phase dephasing for the phase-only configuration of the LCSLM.

SLM this effect can be considered an apodization on the plane of the lens. Next we experimentally demonstrate this inherent equivalent apodizing effect when the DOE acts as a focusing lens.

3. Experimental Setup

In our experiments we encoded a quadratic phase pattern as in Eq. (1) onto a LCSLM that represents the lens with a circular pupil. We used a twisted nematic LCSLM Sony panel (Model LCX012BL) extracted from Sony Video projector Model VPL-V500. This device has 640 × 480 square pixels with a pixel spacing D of 41 μm and a pixel width W of 34 μm. The panel was illuminated with the expanded and collimated 488-nm wavelength output from an argon laser.

Phase-only operation for a twisted nematic LCD can be achieved by use of a combination of two polarizers (LP's) and two quarter-wavelength plates (QWP's).[7] We achieve excellent phase-only operation for our device when the input polarizer is at 40° relative to the slow axis of the input wave plate and the output polarizer is at −16° relative to the slow axis of the output QWP. The slow axes of the wave plates are aligned parallel to the director axes of the LCSLM at both faces. The amplitude and phase modulation values provided by our device in this configuration are shown in Fig. 1. We achieve an amplitude transmission that is uniform within 5% and a phase range of nearly 2π rad, which constitute excellent operating curves for generating DOE's. Using our phase-modulation curve, we generated a calibration phase versus gray-level look-up table.

The experimental setup needed for generating the lens on the LCSLM is shown in Fig. 2. Note that the LCSLM is inserted between the two sets of LP's and QW's to achieve phase-only operation. A quadratic phase function that represents a lens with a focal length of 1 m and an aperture diameter of 300 pixels is written onto the LCSLM. With this focal length we are within the limit of the Nyquist frequency, and no secondary lenses appear. The focused spot is magnified with a 10× microscope objective (MO) and imaged onto a CCD camera. To examine various defocus planes, we fix the distance d_{MO} between the microscope objective and detector and move the entire objective–detector system.[8]

4. Experimental Results

A. Experimental Measurement of the Inherent Apodizing Effect

To measure the inherent apodizing effect that exists in the lens that is displayed on the LCSLM, we used the setup shown in Fig. 2. We experimentally measured the apodizing function τ(ρ), where ρ represents the radial coordinate in the SLM plane, by programming annular rings that had different central radii and areas into the lens function and measuring the focused intensity from each ring. In Fig. 3 we show one of the programmed annular rings, in which the central radius ρ_R is marked. In the clear area of the ring we can see the encoded lens. For these experiments the quadratic phase function was encoded inside the annular ring while a constant phase was encoded for the remaining region of the lens. Let us see in what follows how the apodizing function τ(ρ) is related to the intensity at the center of the focal spot produced by these rings.

Amplitude $U(r = 0)$ in the center of the focal plane

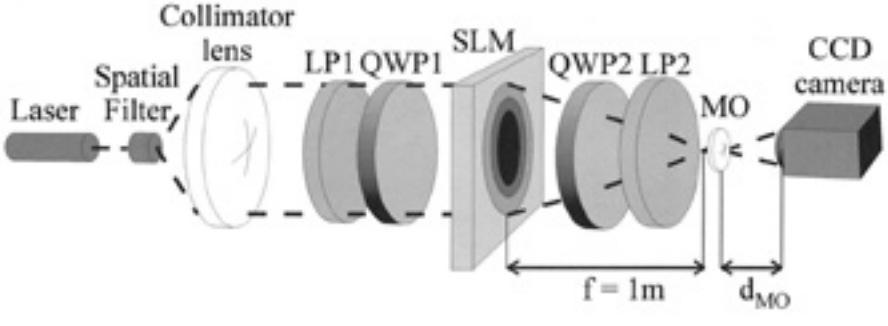

Fig. 2. Optical setup: f, focal length; other abbreviations defined in text.

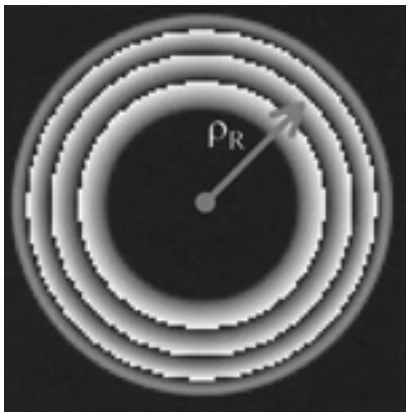

Fig. 3. Annular ring with central radius ρ_R, where we can see the encoded lens.

(r is the radial coordinate in the focal plane) of an optical system without aberrations is given by

$$U(r = 0) = \iint_R \tau(\rho, \phi)\rho d\rho d\phi, \tag{10}$$

where (ρ, ϕ) are the polar coordinates in the pupil plane and $\tau(\rho, \phi)$ is the amplitude transmission of the pupil. The integral is extended to pupil region R. For radial symmetry, Eq. (10) becomes

$$U(r = 0) = 2\pi \iint_R \tau(\rho)\rho d\rho. \tag{11}$$

In our case the pupil is a ring with central radius ρ_R. We consider the annular ring with a width small enough that $\tau(\rho)$ is almost constant inside the area A of the ring. Then from Eq. (11) we obtain

$$U(r = 0) = A\tau(\rho_R). \tag{12}$$

Experimentally we measure the intensity in the center of the focal plane, $I(r = 0)$. As the intensity is the square of amplitude $U(r = 0)$ and by taking Eq. (12) into account, we can extract the value of $\tau(\rho_R)$ as follows:

$$\tau(\rho_R) = \sqrt{I(r = 0)}/A. \tag{13}$$

If the apodizing effect were not present $[\tau(\rho_R) = 1]$, these annular rings would yield focused intensities that are proportional to the square of the areas of the annular rings. But with the apodization effect these intensities will be proportional to the product of the square of the area of the annular rings and the square of the apodizing function. Then, by measuring the intensities produced by annular rings centered in different radii ρ_R, we are able to deduce the inherent apodization function $\tau(\rho_R)$. In Fig. 4 we show the equivalent amplitude distribution $\tau(\rho_R)$ calculated from the experimental intensity measurements obtained for nine different annular rings. As expected, the amplitude in the center of the focal plane decreases as the radius increases, a result that is indicative of the apodizing effect. These measurements confirm the existence of an equivalent nonuniform transmission pupil that will produce an apodization of the point-spread function of the focused spot. The experimental data were fitted to a parabola as $\tau_P(\rho) = 0.97423 - 0.00894\rho^2$ that is also represented in Fig. 4.

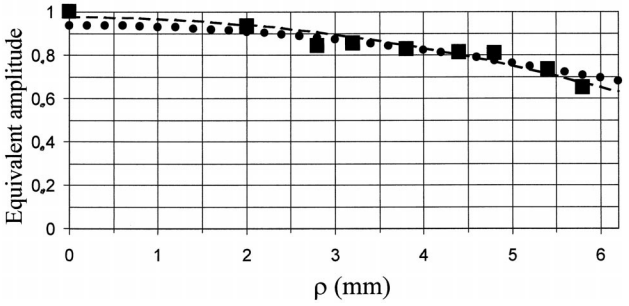

Fig. 4. Apodizing effect of the LCSLM along the radius of the lens. Experimental points measured with annular masks (filled squares), sinc fitting (filled circles), and parabolic fitting (dashed curve).

To compare these experimental results, we evaluated Eq. (7) with the dimensions of the pixels. The two-dimensional pupil function is given by $\tau(u, v) = C\,\mathrm{sinc}(0.07u)\mathrm{sinc}(0.07v)$, where u and v are expressed in millimeters. An angular average of this curve is also represented in Fig. 4. The average of the square differences between the experimentally measured nine points and the corresponding theoretically calculated points is 0.0012, which represents good agreement between the theoretical and the experimental results.

In Fig. 5 the numerically calculated intensity distribution of the focused spot is shown for a clear-aperture pupil and for a pupil with an aperture with the radial apodizing effect $[\tau_P(\rho)]$. Figure 5(a) shows that the apodizing effect decreases the intensity of the first sidelobe and slightly shifts the position in the first zero of the intensity distribution. Figure 5(b) shows that the apodizing effect increases the mini-

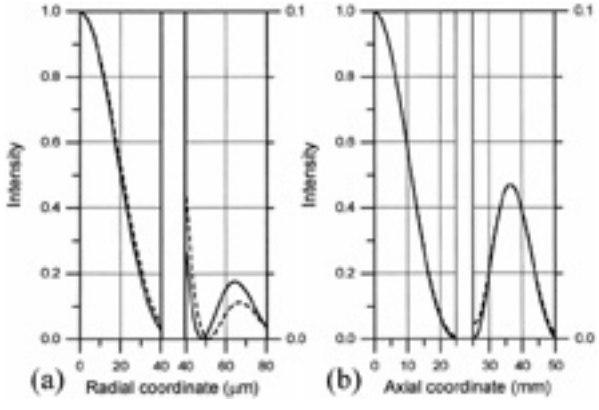

Fig. 5. Theoretically calculated intensity for lens behavior (a) in the best image plane and (b) in the axial direction. Lens with no apodizing effect, solid curves; lens with apodizing effect, dashed curves.

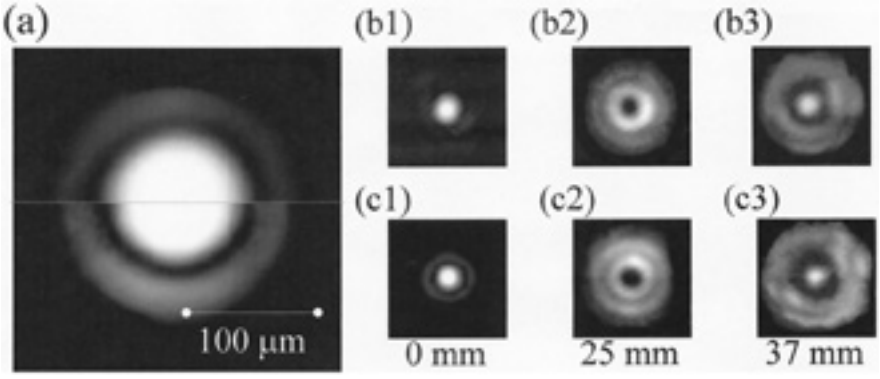

Fig. 6. Experimental measurements of the intensity of the focused spot. (a) Combination of saturated images in the best image plane (upper half, encoded lens; lower half, compensated lens). (b), (c) Planes at different axial positions produced by the encoded lens and the compensated lens: best image plane, (b1), (c1); first minimum planes, (b2), (c2); first maximum planes, (b3), (c3).

mum intensity along the axial coordinate but does not affect the positions of the first minimum and the first maximum. In Subsection 4.B we will see a comparison with experimental results.

B. Correction of the Apodizing Effect

As we have shown, the lenses that are encoded in a pixelated SLM have an inherent apodizing effect. Usually the pixel shape is rectangular. Consequently, the apodization is not circularly symmetric. The apodization diminishes the secondary maxima of the point-spread function but increases the width of the central lobe. Consequently the resolution of the system decreases. In some situations these effects are not convenient, and compensation for the apodization is required. To compensate for this apodizing effect, one should use a filter with an amplitude transmission $\tau_I(\rho)$ equal to the inverse function of Fig. 4. However, doing so would require a second SLM that would incorporate the amplitude transmission function.

An easier alternative is to encode this amplitude modulation function as a phase modulation. One of the earliest methods for doing this was described by Kirk and Jones,[9] but it is extremely difficult to implement, particularly with SLM's, because of the need for a high-frequency carrier. We are going to use a recent method proposed by Davis *et al.*[10] that is especially suitable for SLM's and other low-spatial-frequency devices. We begin with the desired complex transmission function that combines the quadratic phase function $\exp[-i\phi_Q(\rho)]$ and amplitude modulation $\tau_I(\rho)$ as

$$T(\rho) = \tau_I(\rho)\exp[-i\phi_Q(\rho)]. \tag{14}$$

As shown in Ref. 10, we can obtain this transmission function, using a phase-only SLM, by encoding a phase function given by

$$T'(\rho) = \exp[-i\tau'_I(\rho)\phi_Q(\rho)]. \tag{15}$$

As the depth of the phase distribution is spatially modified by the transmission function, the diffraction efficiency of the lens is spatially modulated. In regions where the transmission function is low, the amount of light focused into the original focal plane will decrease. This light will not be absorbed as in a conventional transmitting filter; instead, it will be focused into other focal planes. This technique has been demonstrated successfully for the implementation of classic and matched spatial filters as well as for inverse filters for pattern recognition.

The phase distribution of Eq. (15) can be represented as a mixed Fourier–Taylor series[10,11] as

$$T'(\rho) = \sum_{n=-\infty}^{\infty} T'_n(\rho)\exp[-in\phi_Q(\rho)], \tag{16}$$

where the new coefficients $T'_n(\rho)$ are given by

$$T'_n(\rho) = \frac{\sin\{\pi[n - \tau'_I(\rho)]\}}{\pi[n - \tau'_I(\rho)]}. \tag{17}$$

The first-order term in Eq. (16) reproduces the desired complex transmission function and will focus light into the original focal plane. There is some distortion caused by the sinc function in Eq. (17), but it is compensated for by use of a look-up table that makes $T'_1(\rho) = \tau_I(\rho)$. The remaining diffraction orders are encoded with lenses that have different focal lengths of $\pm f/n$ and will be focused into different planes. In the plane where the first order is focused, the unwanted orders will be out of focus and will have a lower intensity. Consequently, the unwanted orders yield a background noise that is not important. In a computer simulation, we obtained that the ratio between the intensities in the background and in the center of the focal spot is 0.005. In the case when an extended object is imaged, further research to study the contrast in the image plane is needed.

In Fig. 6 the experimental results are shown with the lens encoded in the LCSLM (in which the apodizing effect is apparent) and with the compensated lens encoded in the LCSLM (in which the apodizing effect is compensated).

Figure 6(a) shows the focused spot from the encoded lens (top) and for the lens in which the apodizing effect is compensated for (bottom). The shift in the position of the first minimum and the lower intensity of the first

secondary maximum show the apodizing effects of an encoded lens in a LCD. The radius of the first minimum in the lower part of Fig. 6(a) corresponds to the radius of the free aberration system with the clear-aperture size of the designed lens.

The rows of images in Figs. 6(b) (apodized) and 6(c) (corrected apodization) show three different transverse images produced by the lens encoded directly in the LCSLM. Images 6(b1) and 6(c1) correspond to the best image plane. We can see that, in the directly encoded lens, the first secondary maximum has almost disappeared as a result of the apodizing effect. Figures 6(b2) and 6(c2) correspond to the first minimum along the axis (located at 25 mm as predicted numerically), and Figs. 6(b3) and 6(c3) correspond to the first secondary maximum along the axis (located at 37 mm, as predicted numerically).

We note that the images in Fig. 6 are not totally symmetric, probably because of the existence of aberrations produced by the different elements (polarizers, wave plates, lenses) in the setup. In fact, the modulator that we are using is almost free from aberrations and allows us to obtain diffraction-limited images. For SLM's that introduce phase aberrations, further research to study ways to compensate for the aberrations will be required.

5. Conclusions

We have shown experimentally an apodizing effect that is inherent in the encoding of a lens in a LCSLM. We have also proposed a method to compensate for it by using a phase-modulation technique to encode the complex transmission function. Consequently, both the quadratic phase function and the function that compensates for the apodizing effect can be encoded simultaneously in the same phase-only SLM. Experimental results show that this apodizing effect can be removed.

This study is financed by Direccion General de Enseñanza Superior del Ministerio de Educación y Cultura project PB96-1134-C02-01 and by the Programa de Cooperación Científica con Iberoamérica (Spain). A. Márquez thanks the Comissionat per a Universitats i Recerca de la Generalitat de Catalunya (Spain) for a grant. C. Iemmi and S. Ledesma thank the Consejo Nacional de Investigaciones Científicas y Técnicas and Universidad de Buenos Aires (Argentina).

References

1. F. Wyrowski, and O. Bryngdahl, "Digital holography as part of diffractive optics," Rep. Prog. Phys. **54,** 1481–1571 (1991).
2. J. A. Davis, D. M. Cottrell, R. A. Lilly, and S. W. Connely, "Multiplexed phase encoded lenses written on spatial light modulators," Opt. Lett. **14,** 420–422 (1989).
3. D. M. Cottrell, J. A. Davis, T. R. Hedman, and R. A. Lilly, "Multiple imaging phase-encoded optical elements written as programmable spatial light modulators," Appl. Opt. **29,** 2505–2509 (1990).
4. K. J. Weible and H. P. Herzig, "Optical optimization of binary fan-out elements," Opt. Commun. **113,** 9–14 (1994).
5. E. Carcolé, J. Campos, and S. Bosch, "Diffraction theory of Fresnel lenses encoded in low-resolution devices," Appl. Opt. **33,** 162–174 (1994).
6. V. Arrizon, E. Carreon, and L. A. Gonzalez, "Self-apodization of low-resolution pixelated lenses," Appl. Opt. **38,** 5073–5077 (1999).
7. J. A. Davis, I. Moreno, and P. Tsai, "Polarization eigenstates for twisted-nematic liquid-crystal displays," Appl. Opt. **37,** 937–945 (1998).
8. J. A. Davis, J. C. Escalera, J. Campos, A. Marquez, M. J. Yzuel, and C. Iemmi, "Programmable axial apodizing and hyperresolving amplitude filters with a liquid-crystal spatial light modulator," Opt. Lett. **24,** 628–630 (1999).
9. J. P. Kirk and A. L. Jones, "Phase-only complex-valued spatial filter," J. Opt. Soc. Am. **61,** 1023–1028 (1971).
10. J. A. Davis, D. M. Cottrell, J. Campos, M. J. Yzuel, and I. Moreno, "Encoding amplitude information onto phase-only filters," Appl. Opt. **38,** 5004–5013 (1999).
11. W. J. Dallas, "Computer Generated Holograms," in *The Computer in Optical Research,* B. R. Frieden, ed., Vol. 41 of Topics in Applied Physics Series (Springer-Verlag, Berlin, 1980), Chap. 6.

Amplitude apodizers encoded onto Fresnel lenses implemented on a phase-only spatial light modulator

Andrés Márquez, Claudio Iemmi, Juan C. Escalera, Juan Campos, Silvia Ledesma, Jeffrey A. Davis, and María J. Yzuel

We show that both a lens and a nonuniform amplitude transmission filter can be encoded simultaneously onto a twisted nematic liquid-crystal spatial light modulator (SLM) working in the phase-only mode. The inherent equivalent apodization that is due to the pixelated structure of the SLM is compensated for. In addition, different types of nonuniform transmission pupil such as transverse apodizing, transverse hyperresolving, and axial hyperresolving (multifocusing) filters are implemented. The excellent agreement between numerical and experimental results shows the capability of this method to encode amplitude apodizers on a phase-only SLM. © 2001 Optical Society of America

OCIS codes: 230.3720, 120.4820, 110.2990, 260.1960.

1. Introduction

The use of spatial light modulators (SLMs) to implement diffractive optical elements (DOEs) has been reported to be a useful tool in real-time optical processing.[1–3] For example, if we want to display a lens, a spherical wave must be encoded on the SLM, and we can dynamically change the lens's focal length during the experiment.

For Fresnel phase-encoded lenses the low resolution of the device produces the appearance of secondary maxima in the focal plane with a loss of efficiency in the principal focus. As has been reported by Cottrell *et al.*,[3] this effect increases as the focal length decreases. Carcolé *et al.*[4] reported a mathematical model with which to describe low-resolution Fresnel lenses encoded on SLMs, and they calculated the optimal focal length to be encoded to avoid this effect.

An additional effect that is inherent in the pixelated structure of the SLM when a lens is displayed has been reported by Arrizón *et al.*[5] This apodization has its origin in the finite size of the pixels, and it depends on the ratio of the focal length to the size of the pixel. In a recent paper[6] we demonstrated that the pixelated structure of the SLM introduces an apodizing effect that can be corrected by use of an appropriate encoded function that compensates for the apodization.

Twisted nematic liquid-crystal displays (LCDs) have been widely used as SLMs. In general, they produce coupled amplitude and phase modulation relative to the applied voltage. When diffractive optical elements are displayed, phase-only modulation is desired. By using properly oriented linear polarizers or by generating and detecting appropriate elliptically polarized eigenstates,[7,8] one can modulate mainly the phase while the amplitude is kept almost constant. Recently we presented a more general approach[9] that predicts the configuration of the polarizing elements that produces the desired modulation through the use of elliptically polarized light. This approach is based on the physical model for the twisted nematic LCDs proposed in Ref. 10.

When a focusing lens is needed, the most appropriate way to generate that lens is by encoding a quadratic phase onto the LCD working in the phase-only mode. It is well known that nonuniform transmission filters in the pupil can modify the impulse response of the optical system. In some cases the pupil filters are used to modify the transverse response of the system, for example, by producing apodization or hyperresolution.[11,12] At other times the filters are introduced to produce specific axial properties,[13,14] for instance, to increase the depth of focus

A. Márquez, J. C. Escalera, J. Campos (e-mail: juan.campos@uab.es), and M. J. Yzuel are with the Departamento de Física, Universidad Autónoma de Barcelona, 08193 Bellaterra, Spain. J. A. Davis is with the Department of Physics, San Diego State University, San Diego, California 92182. C. Iemmi and S. Ledesma are with the Departamento de Física, Facultad de Ciencias Exactas y Naturales, Universidad de Buenos Aires, (1428) Buenos Aires, Argentina.

Received 19 October 2000; revised manuscript received 29 January 2001.

0003-6935/01/142316-07$15.00/0

or to produce a multifocus effect.[15,16] Finally, we can search for a particular pupil filtering that produces a combined effect in the transverse and axial response, for instance, in a photolithographic system, to produce both transverse superresolution and large focal depth.[17,18] In a previous paper[19] we showed the experimental realization of pupil filters with a liquid-crystal SLM operating in the amplitude-only mode.

In a focusing optical system in which a particular response is desired, the lens can be phase encoded by means of one SLM working in the phase-only mode while another SLM working in the amplitude-only mode displays the nonuniform transmission filter. This optical system can be implemented with two SLMs, but careful alignment of the devices is required. Recently we introduced a technique in which both amplitude and phase can be combined onto a single phase-only SLM.[20]

In this paper we demonstrate that both functions, those of the lens and of the nonuniform pupil, can be encoded on the same SLM working in the phase-only mode. In Subsection 2.A we describe a method for encoding an arbitrary two-dimensional complex function as a phase-only function. We achieve the effect of the lens by adding a quadratic phase. In Subsection 2.B we analyze the apodizing effect that is due to the pixelated structure of the SLM when a lens is displayed. The experimental setup with the twisted nematic LCD working in the phase-only mode is described in Section 3. In Subsection 4.A we show the result of measuring the inherent equivalent apodization that is due to the pixelated structure of the SLM. Once this effect is compensated for, transverse apodizing, transverse hyperresolving, and axial hyperresolving (multifocusing) optical systems yield the numerical and experimental results described in Subsection 4.B. The agreement between theory and experiment is excellent, thus validating the feasibility of our proposal.

2. Theoretical Development

A. Phase Encoding of the Amplitude Filters

To be able to display the lens and the nonuniform amplitude filter in the same SLM, we extended to two dimensions the method proposed by Davis *et al.*[20] for the one-dimensional geometry. This method is based on the encoding of an arbitrary complex function by means of an adequate phase function. Reference 20 describes the addition of a one-dimensional grating to the phase filter to produce the required response. Here we demonstrate that the addition to the complex transmission of the filter of a quadratic phase associated with a lens allows us to obtain the adequate response on the lens's focal plane. We briefly describe the encoding method.

In our case we are interested in displaying a complex filter $T(u, v)$ and a lens in a single SLM working in the phase-only mode. We can represent the complex transmittance of the filter as a function $T(u, v) = M(u, v)\exp[i\Phi(u, v)]$, where $|M(u, v)| \leq 1$ and $-\pi \leq \Phi \leq \pi$. Let $Z^*(u, v)$ be the quadratic phase introduced by a lens with focal length f, illuminated with a plane wave with wavelength λ:

$$Z^*(u, v) = \exp\left[-i\,\frac{\pi}{\lambda f}(u^2 + v^2)\right]. \tag{1}$$

To display both the filter and the lens on the same SLM, we phase encode the complex function:

$$\begin{aligned} G(u, v) &= T(u, v)Z^*(u, v) \\ &= T(u, v)\exp\left[-i\,\frac{\pi}{\lambda f}(u^2 + v^2)\right]. \end{aligned} \tag{2}$$

As in Ref. 20, first we define the phase function $G'(M', \varphi) = \exp(iM'\varphi)$, with $|M'| \leq 1$ and $-\pi \leq \varphi \leq \pi$, where $\varphi = \Phi(u, v) - [\pi(u^2 + v^2)/\lambda f]$. Then we define the periodic extension $G''(M', \varphi)$ of this function by repeating it in the range $-\infty \leq \varphi \leq \infty$. The Fourier expansion of this periodic function will be

$$G''(M', \varphi) = \sum_{n=-\infty}^{n=\infty} G_n \exp(in\varphi), \tag{3}$$

where $G_n = \mathrm{sinc}(M' - n)$, with the usual definition $\mathrm{sinc}(x) = \sin(\pi x)/(\pi x)$. We can rewrite G'' in terms of u and v:

$$\begin{aligned} G''(u, v) = \sum_{n=-\infty}^{\infty} &\mathrm{sinc}[M'(u, v) - n] \\ &\times \exp\left\{in\left[\Phi(u, v) - \frac{\pi(u^2 + v^2)}{\lambda f}\right]\right\}. \end{aligned} \tag{4}$$

If a plane wave with wavelength λ illuminates a SLM where this transmission has been displayed, according to the Fresnel diffraction theory the resultant electric field $U'(x, y)$ on a plane x–y placed at a distance f from the plane u–v will be proportional to

$$\begin{aligned} U'(x, y) \propto &\exp\left[\frac{i\pi(x^2 + y^2)}{\lambda f}\right] \\ &\times \int_{-\infty}^{\infty}\int_{-\infty}^{\infty} \sum_{n=-\infty}^{\infty} \mathrm{sinc}[M'(u, v) - n]\exp\left\{in\left[\Phi(u, v) \right.\right. \\ &\left.\left. - \frac{\pi(u^2 + v^2)}{\lambda f}\right]\right\} \exp\left[\frac{i\pi(u^2 + v^2)}{\lambda f}\right] \\ &\times \exp\left[\frac{-i2\pi(ux + vy)}{\lambda f}\right] du\,dv. \end{aligned} \tag{5}$$

For the term $n = 1$ the quadratic phase is compensated for; then $U'(x, y)$ is the Fourier transform of $\mathrm{sinc}[M'(u, v) - 1]\exp[i\phi(u, v)]$. Additionally, if we choose $G_1(u, v) = \mathrm{sinc}[M'(u, v) - 1] = M(u, v)$, the Fourier transform of the function that has been encoded is obtained. For the other terms ($n \neq 1$), the quadratic phase $\exp[in\pi(u^2 + v^2)/\lambda f]$ is not compensated for. In general, the phase of the n term can be thought to be produced by a lens with a focal length f/n. These terms will appear defocused, and their contribution to $U'(x, y)$ will be almost a constant on

the plane x–y. Moreover, the intensities of these defocused terms are governed by the function $\mathrm{sinc}[M'(u, v) - n]$ and, because $0 \leq M'(u, v) \leq 1$, the main contribution is given by the zero-order term. Even for this term the resultant intensity will be lower than the first-order contribution. Then the resultant intensity on this plane will be the Fourier transform of the function that we have encoded plus a low background noise.

To verify this, we evaluated the signal-to-noise ratio of the intensity when an apodizing function $M(u, v)$ is encoded. We chose $M(u, v) = 1 - (u^2 + v^2/\rho_{\max}{}^2)$, where $\rho_{\max}$ is the lens radius. In this case the signal-to-noise ratio was 1:0.005. This high value shows that the contributions to $U'(x, y)$ of the terms $n \neq 1$ can be neglected.

When we encode a nonuniform transmission function onto the quadratic phase function that corresponds to the lens, the contribution of the first-order term is enhanced at the focal plane of the lens function, whereas the terms in which $n \neq 1$ are defocused. Therefore, at the focal plane of the encoded lens the field distribution produced by the encoded function will be the Fourier transform of the original function immersed in low background noise.

B. Effect of the Pixelated Structure of the SLM

As we showed in a recent paper,[6] the pixelated structure of the SLM can be represented as an inherent equivalent apodizing filter in the lens plane. As the transmission $G'(M', \varphi)$ will be displayed on a pixelated SLM, this additional effect of apodization will be present and will result in a decrease of the secondary maxima of the point-spread function and in an increase of the width of the central lobe. In many situations these could be undesirable effects, and a correction to compensate for the equivalent inherent apodizing effect must be introduced.

As is shown in Ref. 6, the transmission $\tau(u, v)$ in the lens plane that is due to the pixelated structure of the SLM is equivalent to a product of two sinc functions that correspond to the Fourier transform of the pixels,

$$\tau(u, v) = \mathrm{sinc}(Wu/\lambda f)\mathrm{sinc}(Wv/\lambda f), \qquad (6)$$

where W is the pixel size in both directions u and v, f is the distance from the lens to its focal plane, and λ is the wavelength of the incident light beam. This equivalent nonuniform transmission pupil in the lens plane accounts for the apodizing effect on the point-spread function. Note that, when the pixel size tends to zero, this effect is negligible; however, it becomes more noticeable as the pixel size increases. In addition, for a fixed pixel size the effect of the apodization increases when the focal lens decreases. We correct the equivalent apodizing effect by multiplying the transmission of the desired filter $T(u, v)$ by the inverse function $\tau_I(u, v)$ of Eq. (6). In this case we shall have a new amplitude transmission that can be encoded by the method described in Subsection 2.A. The inverse function $\tau_I(u, v)$ is calculated with the condition that $\tau(u, v)\tau_I(u, v) = k$, where k is a constant. To maximize the transmission of the inverse function $\tau_I(u, v)$ we set k equal to the minimum transmission value of $\tau(u, v)$ in Eq. (6).

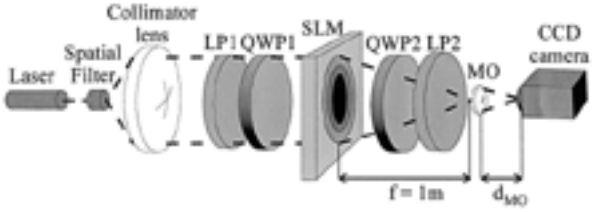

Fig. 1. Optical setup: LPs, linear polarizers; WPs, wave plates; MO, microscope objective.

3. Experimental Optical System with a Phase-Only SLM

To implement the different optical systems we use the experimental setup shown in Fig. 1. Light from an argon laser with a wavelength of 458 nm is filtered, expanded, and collimated. Then it is sent through SLM that has been inserted into an architecture of polarizing devices, as described in Ref. 9, that permits the generation and detection of any state of elliptically polarized light. This architecture consists of a combination of an input polarizer and a wave plate in front of the SLM and an output wave plate and a polarizer behind the SLM. The focused spot is magnified with a 20× microscope objective and imaged onto a CCD camera. The microscope objective also serves as a spatial filter to eliminate higher-order diffracted images caused by the pixel structure of the SLM. To examine various defocus planes, we fix the distance d_{MO} between the microscope objective and the detector and translate the entire objective–detector system. The Fresnel lens implemented in the SLM has a focal length of 1 m and a radius of 204 pixels.

In our experiments we use a Sony LCX012BL twisted nematic LCD SLM extracted from a Sony Model VPL-V500 video projector. We used previously discussed techniques[21–23] to measure the operating parameters of the LCD. For our device the orientation of the director axis angle at the entrance face with respect to the vertical of the lab is +46 deg, the twist angle is −92 deg, and the value of the birefringence when the liquid-crystal cell is in the off state is 231 deg for a wavelength $\lambda = 458$ nm. This video projector has a video graphics array resolution of 640 × 480 pixels with square pixels that have a side size W of 34 μm and are separated by a distance D of 41.3 μm.

The phase retardance values introduced by the input and the output wave plates are, respectively, 125 and 95 deg. We used the procedure described in Ref. 9 to predict a configuration that provides phase-only modulation. The result for a flat intensity transmission leads to 26- and 0-deg angles of the transmission axis of the input polarizer and of the slow axis of the input wave plate, respectively, with respect to the

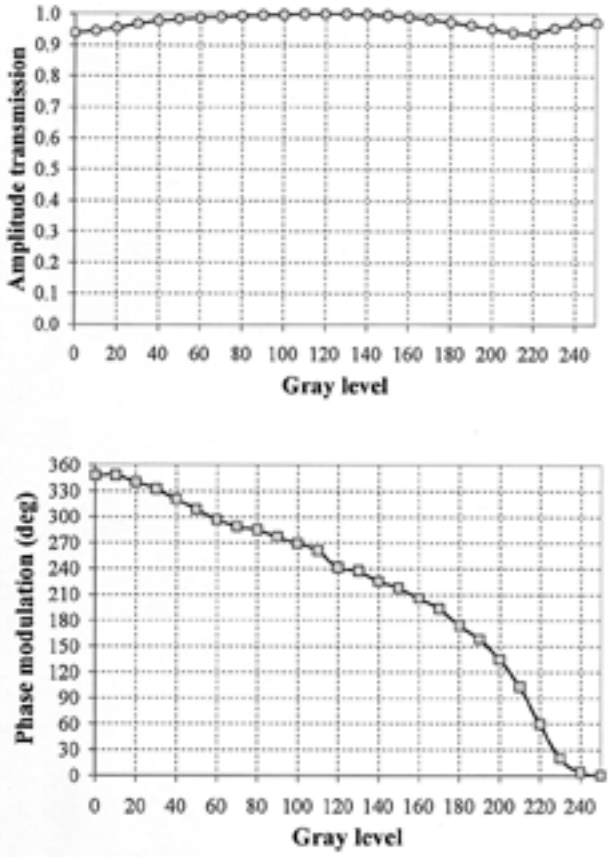

Fig. 2. Normalized amplitude transmission and phase dephasing for the phase-only configuration of the SLM.

director axis in the input face of the SLM and to −16 and 11-deg angles of the transmission axis of the output polarizer and of the slow axis of the output wave plate, respectively, with respect to the director axis in the output face of the SLM. Figure 2 shows the normalized amplitude transmission and the phase dephasing measured with this configuration. We can see that the phase depth is nearly 2π rad with a variation in the amplitude transmission of as little as 6% over the entire range of gray levels. As discussed in Ref. 9, these are excellent values, particularly for a thin twisted nematic LCD. We generated a calibration phase–versus–gray level look-up table by using the phase-modulation curve.

4. Numerical and Optical Results

A. Correction of the Inherent Apodizing Effect

The lens displayed in our experiment has a focal length of 1 m and a radius of 204 pixels, and the wavelength of the incident light is 458 nm. With these values and using Eq. (6), we find a value of 0.074 mm^{-1} for the constant $(W/\lambda f)$ of the sinc functions as a result of the apodizing effect. In Ref. 6 we proposed a procedure that permits an experimental measurement of the inherent apodizing effect. It consists in multiplying the displayed lens by a series of concentric binary transmission annuli masks and

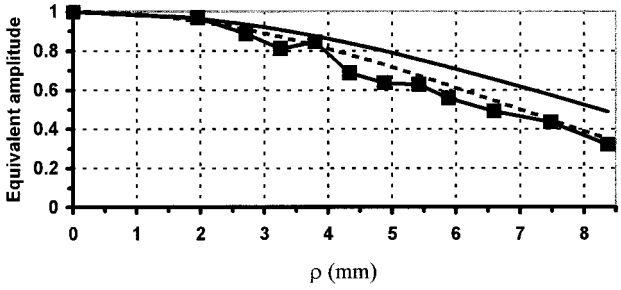

Fig. 3. Amplitude distribution along the radius of the lens (in millimeters). Theoretical simulation of the apodizing inherent equivalent effect that is due to the pixelated structure of the SLM (continuous curve), experimentally measured values with the annuli masks (squares), and polynomial fitting to the experimental values (dashed curve).

measuring the intensity maximum in the focal plane of the lens for each of the annuli masks. From these measurements we extract the equivalent amplitude transmission distribution in the plane of the lens. In Fig. 3 we show the equivalent amplitude transmittance along the radius of the lens obtained from these experimental measurements (squares). The continuous curve corresponds to the angular average of the theoretically expected amplitude transmission calculated with Eq. (6). The experimentally measured intensity is slightly lower than the theoretical values expected with the inherent apodization effect. The difference between experiment and theory is due to the presence of aberrations in the system. The effect of the aberrations is to send light to the sidelobes, thus producing an intensity value in the maximum that is lower than expected.

To compensate for this inherent equivalent apodization in the plane of the lens we follow the procedure proposed in Ref. 6. First, we calculate the polynomial $\tau_P(\rho)$ that fits the experimentally measured transmission, which is given by

$$\tau_P(\rho) = 1 - 0.89\rho^2 + 0.27\rho^4 - 0.04\rho^6, \qquad (7)$$

where ρ is the normalized radial coordinate in the pupil plane and $\rho = 1$ at the edge of the pupil. This transmittance is displayed in Fig. 3 by a dashed curve. In this figure the radial distance is given in millimeters. The transmission of the inverse of this polynomial is displayed with the lens by the procedure developed in Subsection 2.A. In this way the apodizing effect that is due to the pixelated structure of the SLM is compensated for.

B. Nonuniform Amplitude Filters

In this section we show experimentally that we are able to introduce amplitude transmission filters in a phase-only SLM by using the proposed method. We note that the transmission in the pupil is modified by the inherent equivalent apodizing effect given by Eq. (7). So to obtain the desired transmission we have to multiply the theoretical transmission pupil by the

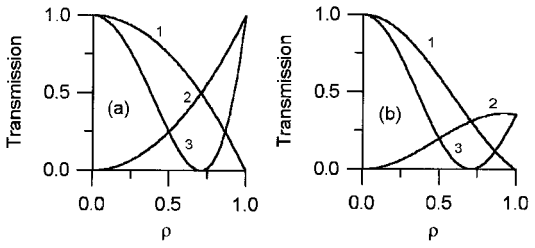

Fig. 4. 1, Transversal apodizing $(1 - \rho^2)$; 2, transversal hyperresolving (ρ^2); and 3, axial multifocusing $(1 - 4\rho^2 + 4\rho^4)$ functions: (a) with no inherent apodizing effect and (b) including the inherent apodizing effect. ρ is the normalized radial coordinate in the plane of the lens.

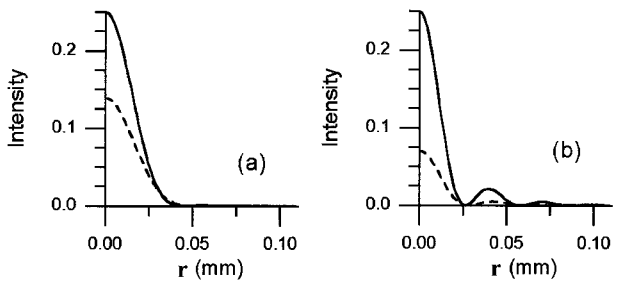

Fig. 5. Theoretical transverse response in the best image plane obtained with (a) a transversal apodizing filter $(1 - \rho^2)$ and (b) a transversal hyperresolving filter (ρ^2). Dashed curves, including the inherent equivalent apodizing effect; solid curves, with no inherent apodizing effect. r is the radial coordinate in the image plane.

inverse of the function that describes the inherent apodizing effect.

To show the wide range of applicability of this new method we selected three filters with widely different features in the best image plane and along the axis. We define three amplitude transmission functions, $T_A(\rho)$, $T_H(\rho)$, and $T_M(\rho)$, as functions of the normalized radial coordinate ρ in the pupil plane for a transversal apodizing, a transversal hyperresolving, and an axial multifocusing system, respectively. The expressions for these transmission functions are

$$\begin{aligned} T_A(\rho) &= 1 - \rho^2, \\ T_H(\rho) &= \rho^2, \\ T_M(\rho) &= 1 - 4\rho^2 + 4\rho^4, \end{aligned} \tag{8}$$

where $\rho = [(u^2 + v^2)/\rho_{\max}{}^2]^{1/2}$ and $\rho_{\max}$ is the radius of a circular pupil displayed in this plane. These desired functions are represented in Fig. 4(a). Figure 4(b) shows the actual transmission functions along the pupil for the filters of Eqs. (8) that include the inherent equivalent apodizing effect described by the polynomial in Eq. (7). So we intend to produce the filters described in Fig. 4(a), but, because of the inherent equivalent apodizing effect, we obtain the filters described in Fig. 4(b). Note that the transmission of the transversal apodizing filter (1) is practically the same in both cases, whereas the hyperresolving filter (2) is greatly distorted relative to the desired filter. The axial multifocusing filter (3) is also distorted.

In Figs. 5(a) and 5(b) we show the theoretically calculated intensity as a function of radial distance r in the best image plane for the apodizing and the hyperresolving filters, respectively. The solid curves show the theoretically calculated intensity as a function of radial distance for the filters from Eqs. (8), and the dashed curves include the inherent apodizing effect described by the polynomial in Eq. (7). We note that in the desirable case (solid curves) the peak intensities are equal, whereas when the inherent equivalent apodizing effect is added (dashed curves) the filter $(1 - \rho^2)$ gives a peak that is twice more intense than the maximum given by the filter ρ^2.

Figure 6 shows the experimental intensity at the best image planes for the two filters. These results are obtained with the setup shown schematically in Fig. 1. Figures 6(a1) and 6(a2) are obtained when we directly send the filters of Eqs. (8) to the SLM and do not compensate for the inherent apodizing effect. Figure 6(a1) corresponds to the apodizing filter, and Figure 6(a2) corresponds to the hyperresolving filter. The theoretical intensity values are shown by dashed curves in Figs. 5(a) and 5(b), respectively. In the experimentally obtained images we can clearly see the apodizing and hyperresolving effects. The central maximum is wider for the apodizing filter than for the hyperresolving filter. The hyperresolving filter produces a secondary maximum [a ring in Fig. 6(a2)] that does not appear with the apodizing filter. These results are in good agreement with the numerical results shown by dashed curves in Fig. 5. The experimental intensity values in the maxima for the apodizing and the hyperresolving filters are 190 and 95, respectively, as shown in Fig. 6. These intensity values are measured in gray levels of the frame grab-

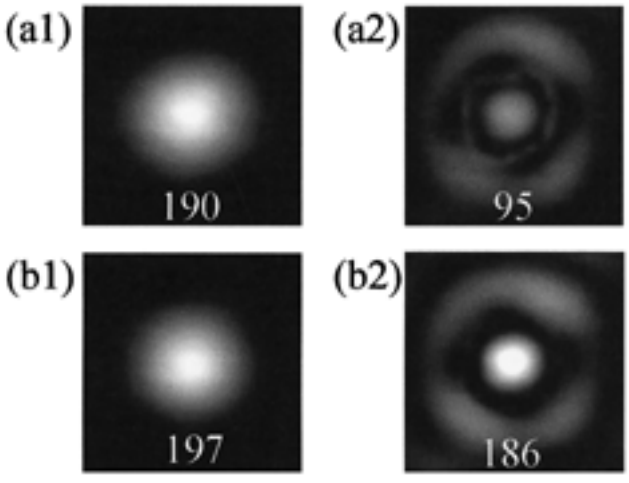

Fig. 6. Experimental best plane images for (a1), (a2), transversal apodizing and transversal hyperresolving filters, respectively, without compensation for the inherent apodizing effect; (b1), (b2), the inherent apodizing effect compensated for. The peak intensity values measured in gray levels of the frame grabber are given.

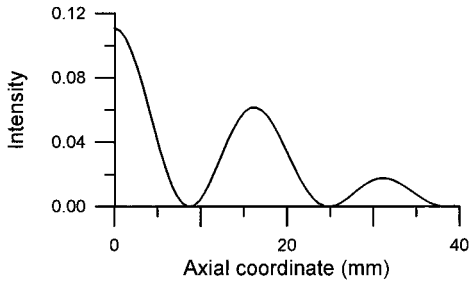

Fig. 7. Axial multifocusing theoretical axial response.

ber. The ratio between them is ~0.5, which coincides with the ratio between the maxima obtained numerically (Fig. 5, dashed curves).

Figures 6(b1) and 6(b2) are obtained when we compensate for the inherent equivalent apodizing effect. Figure 6(b1) corresponds to the apodizing filter, and Fig. 6(b2) corresponds to the hyperresolving filter. Now the intensity at the maximum is practically the same for the two filters, 197 and 186, respectively, as measured with the frame grabber, and it is in good agreement with the numerical results shown in Fig. 5 (solid curves). When the inherent apodizing effect is compensated for, the desired optical response has been recovered.

Next we consider the behavior along the axis of the multifocus filter. In Fig. 7 we display the theoretical intensity response of the multifocus filter $T_M(\rho)$ [see Eqs. (8)] along the axial coordinate z of the system. This filter produces high secondary maxima along the axis. In these planes a good focalization is also obtained.[16]

We study the transverse response in various planes along the optical axis. We show the results in the principal and the first secondary maxima and in the first and the second minima. Taking into account the results from the previous filters, we present only the case when the inherent apodization is compensated for. In Fig. 8 we show the experimental images captured at several defocused planes when the multifocus filter with compensation is displayed. The numerically calculated transverse responses in the corresponding defocused planes are also shown, at the bottom. Radial coordinates are used in the numerically obtained figures. The origin of coordinates ($r = 0$) corresponds to the center of the experimentally obtained results represented by gray-level figures (top). The planes [Figs. 8(a) and 8(c)] show the principal maximum and the first secondary maximum obtained experimentally. These planes were obtained at $z = 0$ and $z = 16.1$ mm. If we look at Fig. 7 we can see that the positions of the two planes are in excellent agreement. Moreover, Figs. 8(b) and 8(d) show the planes where the first and the second axial minimum were experimentally obtained, $z = 8.4$ mm and $z = 24.5$ mm, respectively. These values are also in excellent agreement with the numerical values predicted in Fig. 7. We remark that the experimental images have been saturated to show the sidelobes in the transverse response. In Figs. 8(b) and 8(d), which correspond to the positions of the minima along the axis, the transverse responses appear as rings. This effect agrees with the numerical prediction (bottom of the figure). In Figs. 8(a) and 8(c) we show the values of the gray levels for the peak intensity for the best image plane (200) and for the first secondary maximum (109). The experimental ratio of the intensity of the first secondary maximum to the peak intensity in the best image plane is 0.52, which agrees with the theoretical ratio (0.56).

For all three nonuniform filters, the experimental and computer simulation results are in excellent

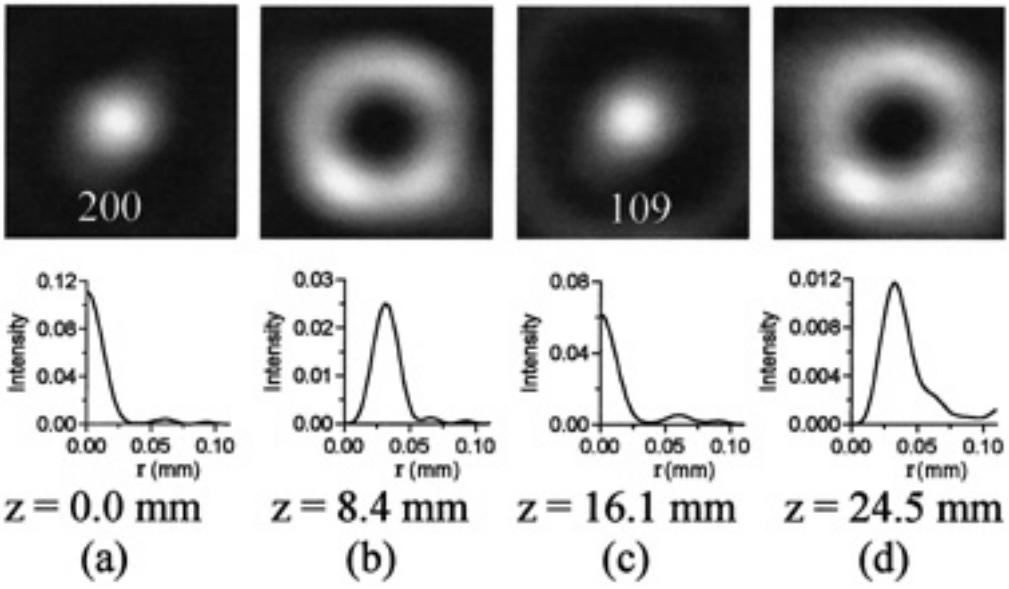

Fig. 8. Axial multifocusing optical system in various defocus planes including compensation for the inherent equivalent apodizing effect. Top, experimental images. Bottom, corresponding numerically calculated transverse responses. r is the radial coordinate in the image plane.

agreement. Once the optical system is properly aligned and the compensating polynomial has been obtained, we can generate the desired optical system, and we can change it in real time, with the SLM working in the phase-only mode.

5. Conclusions

We have shown a new method that demonstrates that both a lens and a nonuniform amplitude transmission filter can be encoded simultaneously onto a phase-only spatial light modulator. The amplitude information is encoded onto the quadratic phase of the lens. We have been able to use a thin twisted nematic liquid-crystal display as an excellent phase-only SLM. The inherent apodization that is due to the pixelated structure of the SLM and the additional effects that are due to the aberrations exhibited by the SLM and the optical system have been measured. When they were compensated for, the desired optical response with the nonuniform amplitude filter was obtained. Any type of nonuniform transmission pupil can be represented. In the research reported in this paper a transverse apodizing, a transverse hyperresolving, and an axial hyperresolving (multifocusing) optical system were implemented. The excellent agreement between numerical and experimental results shows the capability of this method to encode amplitude apodizers on a phase-only SLM.

This research was supported by the Dirección General de Enseñanza Superior del Ministerio de Educación y Cultura (Spain) under project BFM2000-0036-C02-01 and the "Programa de Cooperación Científica con Iberomérica." A Márquez thanks the Comissionat per a Universitats i Recerca de la Generalitat de Catalunya (Spain) for a grant. S. Ledesma and C. Iemmi gratefully acknowledge the support of the Universidad de Buenos Aires and the Consejo Nacional de Investigaciones Científicas y Técnicas (Argentina).

References

1. F. Wyrowsky and O. Bryngdahl, "Digital holography as part of diffractive optics," Rep. Prog. Phys. **54,** 1481–1571 (1991).
2. J. A. Davis, D. M. Cottrell, R. A. Lilly, and S. W. Connely, "Multiplexed phase-encoded lenses written on spatial light modulators," Opt. Lett. **14,** 420–422 (1989).
3. D. M. Cottrell, J. A. Davis, T. R. Hedman, and R. A. Lilly, "Multiple imaging phase-encoded optical elements written as programmable spatial light modulators," Appl. Opt. **29,** 2505–2509 (1990).
4. E. Carcolé, J. Campos, and S. Bosch, "Diffraction theory of Fresnel lenses encoded in low-resolution devices," Appl. Opt. **33,** 162–174 (1994).
5. V. Arrizón, E. Carreón, and L. A. González, "Self apodization of low-resolution pixelated lenses," Appl. Opt. **38,** 5073–5077 (1999).
6. M. J. Yzuel, J. Campos, A. Márquez, J. C. Escalera, J. A. Davis, C. Iemmi, and S. Ledesma, "Inherent apodization of lenses encoded on liquid-crystal spatial light modulators," Appl. Opt. **39,** 6034–6039 (2000).
7. J. A. Davis, I. Moreno, and P. Tsai, "Polarization eigenstates for twisted-nematic liquid-crystal displays," Appl. Opt. **37,** 937–945 (1998).
8. I. Moreno, J. A. Davis, K. G. D'Nelly, and D. B. Allison, "Transmission and phase measurement for polarization eigenvectors in twisted-nematic liquid-crystal spatial light modulators," Opt. Eng. **37,** 3048–3052 (1998).
9. A. Márquez, C. Iemmi, I. Moreno, J. A. Davis, J. Campos, and M. J. Yzuel, "Quantitative prediction of the modulation behavior of twisted nematic liquid crystal displays," submitted to Opt. Eng.
10. A. Márquez, J. Campos, M. J. Yzuel, I. Moreno, J. A. Davis, C. Iemmi, A. Moreno, and A. Robert, "Characterization of edge effects in twisted nematic liquid crystal displays," Opt. Eng. **39,** 3301–3307 (2000).
11. R. Boivin and A. Boivin, "Optimized amplitude filtering for superresolution over a restricted field. I. Achievement of maximum central irradiance under an energy constraint," Opt. Acta **27,** 587–610 (1980).
12. C. S. Chung and H. H. Hopkins, "Influence of nonuniform amplitude on the optical transfer function," Appl. Opt. **28,** 1244–1250 (1989).
13. C. J. R. Sheppard and Z. S. Hegedus, "Axial behavior of pupil-plane filters," J. Opt. Soc. Am. A **5,** 643–647 (1988).
14. J. Campos, J. C. Escalera, C. J. R. Sheppard, and M. J. Yzuel, "Axially invariant pupil filters," J. Mod. Opt. **47,** 57–68 (2000).
15. J. Ojeda-Castañeda, L. R. Berriel-Valdos, and E. Montes, "Ambiguity function as a design tool for high focal depth," Appl. Opt. **27,** 790–795 (1988).
16. M. J. Yzuel, J. C. Escalera, and J. Campos, "Polychromatic axial behaviour of axial apodizing and hyperresolving filters," Appl. Opt. **29,** 1631–1641 (1990).
17. H. Fukuda, Y. Kobayashi, K. Hama, T. Tawa, and S. Okazaki, "Evaluation of pupil-filtering in high-numerical aperture *I*-line lens," Jpn. J. Appl. Phys. **32,** 5845–5849 (1993).
18. R. Hild, M. J. Yzuel, and J. C. Escalera, "High focal depth imaging of small structures," Microelectron. Eng. **34,** 195–214 (1997).
19. J. A. Davis, J. C. Escalera, J. Campos, A. Márquez, M. J. Yzuel, and C. Iemmi, "Programmable axial apodizing and hyperresolving amplitude filters with a liquid-crystal spatial light modulator," Opt. Lett. **24,** 628–630 (1999).
20. J. A. Davis, D. M. Cottrell, J. Campos, M. J. Yzuel, and I. Moreno, "Encoding amplitude information onto phase-only filters," Appl. Opt. **38,** 5004–5013 (1999).
21. C. Soutar and K. Lu, "Determination of the physical properties of an arbitrary twisted-nematic liquid crystal cell," Opt. Eng. **33,** 2704–2712 (1994).
22. J. A. Davis, D. B. Allison, K. G. D'Nelly, M. L. Wilson, and I. Moreno, "Ambiguities in measuring the physical parameters for twisted-nematic liquid crystal spatial light modulators," Opt. Eng. **38,** 705–709 (1999).
23. J. A. Davis, P. Tsai, K. G. D'Nelly, and I. Moreno, "Simple technique for determining the extraordinary axis direction for twisted nematic liquid crystal spatial light modulators," Opt. Eng. **38,** 929–932 (1999).